Phases of cold holographic QCD: baryons, pions and rho mesons

N. Kovensky[1(a)], A. Poole[2(b)], A. Schmitt[3(c)]

1 Institut de Physique Théorique, Université Paris Saclay, CEA, CNRS, Orme des Merisiers, 91191 Gif-sur-Yvette CEDEX, France.
2 Department of Physics and Research Institute of Basic Science, Kyung Hee University, Seoul 02447, Korea.
3 Mathematical Sciences and STAG Research Centre, University of Southampton, Southampton SO17 1BJ, United Kingdom.
(a) nicolas.kovensky@ipht.fr (b) apoole@khu.ac.kr (c) a.schmitt@soton.ac.uk

March 7, 2023

Abstract

We improve the holographic description of isospin-asymmetric baryonic matter within the Witten-Sakai-Sugimoto model by accounting for a realistic pion mass, computing the pion condensate dynamically, and including rho meson condensation by allowing the gauge field in the bulk to be anisotropic. This description takes into account the coexistence of baryonic matter with pion and rho meson condensates. Our main result is the zero-temperature phase diagram in the plane of baryon and isospin chemical potentials. We find that the effective pion mass in the baryonic medium increases with baryon density and that, as a consequence, there is no pion condensation in neutron-star matter. Our improved description also predicts that baryons are disfavored at low baryon chemical potentials even for arbitrarily large isospin chemical potential. Instead, rho meson condensation sets in on top of the pion condensate at an isospin chemical potential of about $9.4\,m_\pi$. We further observe a highly non-monotonic phase boundary regarding the disappearance of pion condensation beyond about ten times nuclear saturation density.

Contents

1 Introduction and conclusions

1.1 Context

Phases of Quantum Chromodynamics (QCD) at non-zero, and not asymptotically large, baryon chemical potential μ_B are notoriously difficult to understand from first principles. In contrast, at non-zero isospin chemical potential μ_I lattice QCD can be employed [1–5]. In this paper we connect – within a single model – the mesonic phases at $\mu_I \gg \mu_B$ with nuclear matter at $\mu_B \gg \mu_I$ and discuss the phases in between, where baryons coexist with meson condensates.

To this end, we employ the Witten-Sakai-Sugimoto (WSS) model [6–8], which is a certain realization of the gauge/gravity correspondence [9, 10], based on the holographic principle. Holographic models have been employed to understand certain aspects of QCD matter that are non-perturbative in nature, for instance in the context of heavy-ion collisions [11, 12]. More recently, they have also increasingly been employed to understand dense baryonic matter in the context of neutron stars [13–22]. Ideally, these calculations would make use of a string dual of QCD. Such a dual, however, is currently unknown, and thus holographic models can provide results for theories similar, but not identical, to QCD. The WSS model is a top-down approach originating from type-IIA string theory. In a certain, albeit inaccessible, limit it is dual to QCD at a large number of colors N_c, and it has proven useful in the discussion of meson, baryon, and glueball spectra and their interactions [23–26] as well as certain properties of QCD matter [27, 28].

Holographic baryonic matter has been studied in different approximations within the (top-down) WSS model [29–36], besides other holographic (bottom-up) approaches [37, 38]. Our main motivation is to improve the recently developed holographic description of isospin-asymmetric baryonic matter [39], which despite its simplicity and shortcomings was shown to yield realistic neutron stars in agreement with astrophysical data [40, 41]. Following the basic setup of these studies, we will work in the background geometry

corresponding to the confined phase, use the Yang-Mills approximation to the Dirac-Born-Infeld action, consider two flavors, and employ the so-called "homogeneous ansatz", where the gauge fields in the bulk are assumed to only depend on the holographic coordinate [30, 32, 34]. This is in contrast to the single-baryon solution of the model, which is a localized instanton in position space as well as in the holographic direction, and whose direct generalization to a many-baryon system is an alternative – somewhat more difficult – description [31–33, 35].

Our main novelties are as follows. Firstly, we include a non-zero pion mass. Due to the geometry of the WSS model, this is more difficult compared to other holographic setups. We shall therefore follow the effective description brought forward in Refs. [42–44] and evaluated in the context of the QCD phase structure (without isospin chemical potential) in Refs. [36, 45]. This improvement allows us to match our holographic results to chiral perturbation theory, compute the onset of pion condensation in the medium of baryonic matter, and determine the pion condensate dynamically throughout the phase diagram. Secondly, when solving the equations of motion in the bulk we use a more general ansatz for the non-abelian gauge fields compared to Ref. [39], where an isotropic approximation was employed. The more general approach renders highly isospin-asymmetric baryonic matter anisotropic, which results in a continuous transition to phases with rho meson condensation, previously discussed in the WSS model only in the absence of baryons [46].

We use this improved description to address various open questions and make model predictions for uncharted territory of the QCD phase diagram. In the region of relatively small isospin asymmetry, $\mu_I \ll \mu_B$, we may ask under which conditions a pion condensate coexists with baryonic matter. The possibility of a p-wave pion condensate in dense nuclear matter and thus the interior of neutron stars was pointed out long ago [47–51], while an s-wave condensate is considered less likely due to the repulsive pion-neutron interaction, although it cannot be ruled out completely [52]. In the opposite limit, where $\mu_I \gg \mu_B$, one may ask whether baryonic states with large isospin number are populated or whether the entire isospin density is generated by mesons. It was conjectured that there is a continuity from pion condensation at low μ_I to Cooper pairs with the same quantum number as the pions at asymptotically large μ_I without the appearance of baryons [53]. Recent studies on the lattice have shed some light on the equation of state at non-zero isospin chemical potential [3, 5], with results including a small baryon chemical potential obtained via Taylor expansion [4], however without conclusive evidence about the (non-)appearance of baryons. These results have been used to speculate about the existence of pion stars [54–56]. Finally, we can extend our results to the region with a sizable μ_B (say comparable to values at the center of neutron stars) and μ_I larger than found in any known astrophysical environment. Although this region might currently be only of academic interest, it may help inform our understanding of the phases in the regions which *are* accessible experimentally or astrophysically.

1.2 Main result

Our main result is the phase diagram in Fig. 1. We will explain the calculation leading to this diagram in the main text and give our conclusions here. The WSS model in the form used here has three parameters, the Kaluza-Klein mass $M_{\rm KK}$, the 't Hooft coupling λ, and the pion mass m_π. We fit these parameters to reproduce the low-density phase transitions of our phase diagram: the $\mu_B = 0$ onset of pion condensation at the physical pion mass $\mu_I = m_\pi = 140\,\text{MeV}$ and the $\mu_I = 0$ baryon onset at $\mu_B = 922.7\,\text{MeV}$. Our fit also ensures that the saturation density of isospin-symmetric nuclear matter and the vacuum mass of the rho meson are reproduced to a good accuracy. As known from previous studies of the model, fitting nuclear matter properties in the given approximation creates tension with

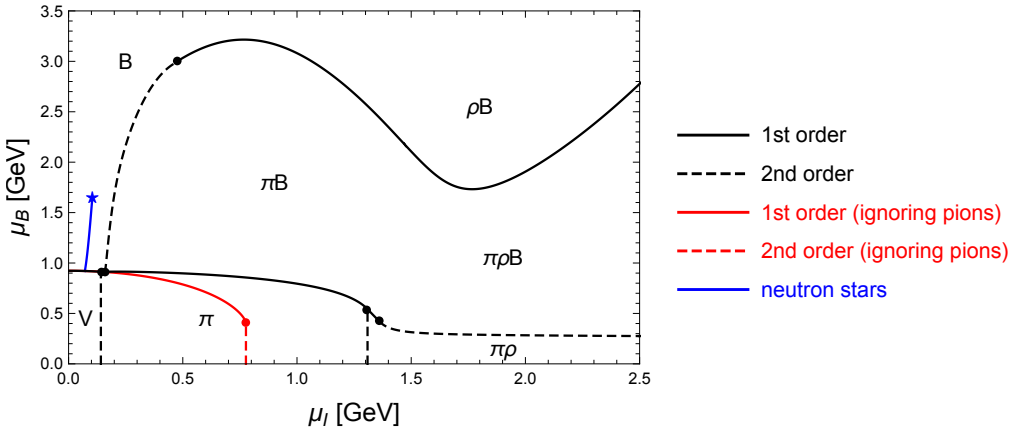

Figure 1: Zero-temperature phase diagram in the plane of baryon and isospin chemical potentials. The various phases are the vacuum (V), the pion-condensed phase (π), the phase where pion and rho condensates coexist ($\pi\rho$), the purely baryonic phase (B) and the phase where baryonic matter coexists with a pion condensate (πB). In both baryonic phases a rho meson condensate develops at large μ_I (in our approximation, the resulting ρB and $\pi\rho$B phases are not distinguished by a phase transition). The red curves show, for comparison, the phase structure in the absence of pion condensation. They separate the vacuum from the B (and Bρ) phase. The blue curve is β-equilibrated, electrically neutral matter relevant for neutron stars, with the marker at the endpoint indicating the chemical potentials in the center of the maximum mass star.

some vacuum properties. Here we need to live with a pion decay constant that is about 30% smaller than its physical value.

The main observations are as follows.

- *Rho meson condensation with pions switched off.* The phase transition lines with pion condensation artificially turned off (red) show the usual first-order baryon onset at $\mu_I = 0$ from the vacuum to isospin-symmetric nuclear matter (the black and red lines are on top of each other for the V-B transition). At $\mu_B = 0$, we have a second-order transition at $\mu_I = 776\,\mathrm{MeV}$, which corresponds to the mass of the rho meson. The resulting phase with rho meson condensation is necessarily anisotropic because the rho meson is a vector meson. Within our approximation, this phase is continuously connected to the baryonic phase. The reason is that in our approximation isospin and position space are coupled and thus any non-zero μ_I creates an anisotropy in our solution. This anisotropy is small at small μ_I (purely baryonic phase) and becomes maximal – in the absence of pion condensation – only at exactly $\mu_B = 0$ (pure rho meson phase).

- *No baryons at small μ_B for any μ_I.* At sufficiently small μ_B, the pion-condensed phase (π) is superseded by a phase where pion and rho condensates coexist. The second-order onset of rho meson condensation in the pionic medium is at $\mu_I \simeq 9.4\, m_\pi$. This is in agreement with Ref. [46]. This reference worked in the chiral limit, but nevertheless observed approximately the same critical chemical potential since the pion mass is negligible in this regime. The second, more fundamental, difference to this reference is that our calculation shows that the $\pi\rho$ phase is indeed preferred over a baryonic phase. *A priori*, it is conceivable that baryons appear for large μ_I even though μ_B is small because they may contribute to the isospin

density. In fact, this was observed in Ref. [39] within the same model, where the approximate isotropic solution was extrapolated to large μ_I. Here, allowing for anisotropic solutions, we conclude that our previous approximation underestimated the free energy of the baryonic phase (i.e., made the highly asymmetric baryonic phase more favorable), and that the model actually predicts a finite band at low μ_B that is purely mesonic. Interestingly, this band only exists if pions are taken into account.

- *Nuclear matter delays pion condensation.* In our holographic baryonic matter, the onset of pion condensation occurs at a *larger* critical chemical potential μ_I than in the vacuum. This observation is in qualitative agreement with an earlier holographic study using a bottom-up approach [37]. (Due to this shift in the onset, there is a small segment – barely visible in the figure – of a direct transition from the π to the B phase.) As a consequence, we find that nuclear matter under neutron star conditions (requiring electroweak equilibrium and electric charge neutrality) does not exhibit pion condensation, in accordance with the predicted absence of s-wave condensation from more traditional approaches. This provides another improvement on Ref. [39], where due to the absence of a pion mass, pion condensation set in immediately at $\mu_I > 0$. It validates *a posteriori* the assumption used in our construction of neutron stars from holography [40], where pion condensation was omitted. We have used the construction of this reference to compute the chemical potentials in the center of the most massive star, which is indicated in the phase diagram[1]. (This calculation includes the holographic construction of the crust of the star and thus, following Ref. [40], uses the surface tension of nuclear matter as an additional input parameter, which we have set to $\Sigma = 1\,\mathrm{MeV/fm^2}$.) Moreover, for all μ_I we consider, the pion condensate vanishes for sufficiently large μ_B. This can only be observed in our improved description with anisotropic baryons and a non-zero pion mass.

- *Curious behavior for large μ_B and μ_I.* The onset of pion condensation in the baryonic medium eventually turns into a first-order transition. At very large μ_I and μ_B there is a very pronounced non-monotonicity in this B-πB transition. We are not aware of any other model calculation to compare this result with and there is no experimental or astrophysical data for this extreme regime. The non-monotonicity occurs at values of μ_I around the rho meson mass in the pionic medium and can thus be related to rho meson admixtures in the B and πB phases, denoted by ρB and $\pi\rho$B in the phase diagram. We will demonstrate that the non-monotonicity disappears for large values of the 't Hooft coupling. In any case, for extremely large chemical potentials we have to interpret the results with care since our probe brane approximation breaks down and, moreover, in real-world QCD we expect deconfinement and chiral transitions, which in our setup are absent.

1.3 Outlook

Our work is a step towards more realistic holographic baryonic matter, in particular clarifying the connection to meson condensation at non-zero isospin chemical potential. Various improvements and extensions are possible in future work. One may perform an analogous calculation in the deconfined geometry of the model, which would give rise to a nontrivial temperature dependence and thus our phase diagram can in principle be generalized by

[1] Pion stars (with electric neutrality and electroweak equilibrium) are located on the μ_I axis with maximal values of μ_I very close to the pion mass, see Table I of Ref. [55].

adding temperature as a third axis. This might be of relevance for a more detailed comparison with lattice results at $\mu_B = 0$, and in the astrophysical context it would provide an equation of state applicable for conditions in neutron star mergers, where zero temperature is no longer a good approximation. The deconfined geometry also provides a deviation from chiral perturbation theory already in the purely pionic phase [39], which is a further motivation to include a non-zero pion mass in this computationally more difficult setting.

Furthermore, it is known that the symmetry energy of holographic nuclear matter in the present approach is unphysically large due to the classical treatment of the isospin spectrum, which is continuous in the large-N_c limit [39]. Recently, a quantization of the homogeneous ansatz has been proposed [57] and it would be interesting to study the effect of this improvement on our phase diagram. Our approach also ignores the possibility of an anisotropic pion condensate, which would be desirable to include for a comparison with predictions of p-wave condensation in neutron star matter. This could be included in the holographic setup by a different choice of boundary conditions, as done in Refs. [58, 59] in the presence of a magnetic field. In the neutron star context it would also be very interesting to consider kaon condensation [60, 61] instead of or possibly in coexistence with pion condensation. This would require the generalization to three flavors which, as a first step, could be done in the mesonic sector only, before including baryons with strangeness in a second step.

1.4 Structure of the paper

Our paper is organized as follows. We present our holographic setup and discuss its relation to chiral perturbation theory in Sec. 2. Important ingredients of the setup compared to earlier work are the chiral rotation discussed in Sec. 2.1 and the mass correction discussed in Sec. 2.2. In Sec. 3 we introduce our holographic baryonic matter and derive the equations of motion, the free energy, and the minimization conditions for the various dynamical parameters. These results are used in Sec. 4 to discuss the different solutions and their interpretation as distinct physical phases. Sec. 5 is devoted to the numerical evaluation: We explain the parameter fit in Sec. 5.1, and while the main results have already been discussed in the introduction, we present a more detailed analysis in Secs. 5.2 – 5.5.

2 Setup and holographic pion condensation

We start by reviewing pion condensation at non-zero isospin chemical potential within chiral perturbation theory [62, 63], and how it is reproduced from the holographic perspective. This will be useful to establish notation, to explain the particular chiral rotation which we shall apply for convenience, and to introduce the mass term, which will be added to our holographic action to effectively account for a non-zero pion mass.

2.1 Pion condensation from the chiral Lagrangian

Two-flavor QCD in the massless limit is invariant under the global chiral symmetry group $U(2)_L \times U(2)_R$. In the real world, where quarks are massive, this symmetry is only approximate (and the axial $U(1)_A \subset U(2)_L \times U(2)_R$ is broken due to the chiral anomaly). At low energies, where the perturbative description in terms of the fundamental quark and gluon degrees of freedom becomes inapplicable, chiral symmetry is spontaneously broken down to its diagonal subgroup, $U(2)_L \times U(2)_R \to U(2)_{L+R}$. The low-energy effective theory for the associated pseudo-Goldstone bosons is formulated in terms of the pion and

mass matrices $\Sigma, M \in U(2)$, which transform under the chiral group as

$$\Sigma' = g_L \Sigma g_R^\dagger \,, \qquad M' = g_L M g_R^\dagger \,, \tag{1}$$

where $(g_L, g_R) \in U(2)_L \times U(2)_R$. To leading order in derivatives and in the pion mass, the chiral Lagrangian reads [64, 65]

$$\mathcal{L} = \frac{f_\pi^2}{4} \mathrm{Tr}[D_\mu \Sigma^\dagger D^\mu \Sigma] + \frac{f_\pi^2 B}{2} \mathrm{Tr}[M\Sigma^\dagger + \Sigma M^\dagger] \,, \tag{2}$$

where f_π is the pion decay constant. The mass matrix contains up and down quark masses, $M = \mathrm{diag}(m_u, m_d)$, while B is proportional to the chiral condensate and can be expressed in terms of pion mass and quark mass $m_q \simeq m_u \simeq m_d$ via $m_\pi^2 = 2 m_q B$. In the absence of electromagnetism, the covariant derivative is

$$D^\mu \Sigma = \partial^\mu \Sigma - i \frac{\mu_I}{2} [\tau_3, \Sigma] \, \delta_0^\mu \,. \tag{3}$$

Here and in the following we denote the Pauli matrices by τ_a ($a = 1, 2, 3$). The isospin chemical potential is normalized such that, as we will see shortly, pion condensation occurs at $\mu_I = m_\pi$. The baryon chemical potential comes together with the unit matrix in flavor space and thus drops out of the covariant derivative, i.e., in this section, where we only discuss the mesonic sector, the results do not depend on μ_B. (In the presence of a magnetic field, the chiral anomaly gives rise to a μ_B dependence of the chiral Lagrangian [66, 67].)

The pion field can be parameterized as

$$\Sigma = \frac{1}{f_\pi} (\sigma \mathbb{1} + i \pi_a \tau_a) \,, \tag{4}$$

where the massive mode $\sigma^2 = f_\pi^2 - \pi_a \pi_a$ is frozen and π_a are the three pionic degrees of freedom. Alternatively, we can parameterize

$$\sigma = f_\pi \cos\psi \cos\theta \,, \tag{5a}$$

$$\pi_1 = f_\pi \cos\psi \sin\theta \cos\alpha \,, \tag{5b}$$

$$\pi_2 = f_\pi \cos\psi \sin\theta \sin\alpha \,, \tag{5c}$$

$$\pi_3 = f_\pi \sin\psi \,. \tag{5d}$$

Then, in the static, homogeneous limit and subtracting the vacuum contribution, the free energy density derived from the Lagrangian (2) is

$$\Omega = -\frac{\mu_I^2}{2}(\pi_1^2 + \pi_2^2) - f_\pi m_\pi^2 (\sigma - f_\pi) = -\frac{\mu_I^2}{2} f_\pi^2 \sin^2\theta \cos^2\psi - f_\pi^2 m_\pi^2 (\cos\psi\cos\theta - 1) \,. \tag{6}$$

Upon minimizing Ω with respect to ψ and θ, one finds that the ground state for $\mu_I < m_\pi$ is the vacuum $\theta = \psi = 0$, where the chiral field is $\Sigma = \mathbb{1}$ and the free energy density is $\Omega = 0$. On the other hand, when $\mu_I > m_\pi$, charged pion condensation becomes favored, with a vanishing neutral pion condensate $\psi = \pi_3 = 0$, and

$$\cos\theta = \frac{m_\pi^2}{\mu_I^2} \,, \qquad \Omega = -\frac{f_\pi^2 \mu_I^2}{2} \left(1 - \frac{m_\pi^2}{\mu_I^2}\right)^2 \,, \qquad n_I = -\frac{\partial \Omega}{\partial \mu_I} = f_\pi^2 \mu_I \left(1 - \frac{m_\pi^4}{\mu_I^4}\right) \,, \tag{7}$$

where n_I is the isospin density. For later use we shall denote the pion matrix with vanishing neutral pion condensate by

$$\Sigma_0 = \cos\theta \, \mathbb{1} + i \sin\theta (\tau_1 \cos\alpha + \tau_2 \sin\alpha) \,. \tag{8}$$

Here, in the purely mesonic scenario, the charged pion condensate is given by Eq. (7), while it will be determined dynamically in our holographic calculation in the presence of baryons. In either case, the system is degenerate with respect to the angle α, which corresponds to the $U(1)_{L+R}$ under which the Lagrangian is invariant even in the presence of an isospin chemical potential. We could therefore set α to any convenient value at this point, but we will keep it unspecified for now in order to check explicitly the degeneracy with respect to α within the full holographic calculation.

For reasons explained in Refs. [39, 46, 58] and that will become clear below, in our holographic study it will be useful to apply a chiral rotation (1) such that

$$\Sigma_0' = g_L \Sigma_0 g_R^\dagger = \mathbb{1}\,. \tag{9}$$

We choose

$$g_R = g_L^\dagger \equiv g\,, \tag{10}$$

such that $g^2 = \Sigma_0$, which is satisfied for instance by

$$g = \cos\frac{\theta}{2}\,\mathbb{1} + \frac{i\sin\theta}{2\cos\frac{\theta}{2}}(\tau_1\cos\alpha + \tau_2\sin\alpha)\,. \tag{11}$$

This defines separate left- and right-handed transformations for $U(2)_L$ and $U(2)_R$ matrices. Since in either case the matrices can be written as linear combinations of the Pauli matrices (and the unit matrix), we compute the transformations on $\boldsymbol{\tau} = (\tau_1, \tau_2, \tau_3)$ from (11),

$$\boldsymbol{\tau}'_{R/L} = \begin{pmatrix} \cos\theta\sin^2\alpha + \cos^2\alpha & \sin\alpha\cos\alpha(1-\cos\theta) & \pm\sin\alpha\sin\theta \\ \sin\alpha\cos\alpha(1-\cos\theta) & \cos\theta\cos^2\alpha + \sin^2\alpha & \mp\cos\alpha\sin\theta \\ \mp\sin\alpha\sin\theta & \pm\cos\alpha\sin\theta & \cos\theta \end{pmatrix} \boldsymbol{\tau}\,, \tag{12}$$

where $\tau'_{a,R/L} = g_{R/L}\tau_a g_{R/L}^\dagger$. In the absence of pion condensation, $\theta = 0$, both left- and right-handed transformations become the identity.

In our holographic model, the isospin chemical potential will be introduced through boundary conditions for the temporal components of the gauge fields on the left- and right-handed branes. Therefore, if we want to perform the calculation conveniently in the frame where $\Sigma_0' = \mathbb{1}$, the pion condensate will enter the boundary conditions via the transformation (12).

The choice (10) is clearly not unique. In particular, it differs from the one used in Refs. [39, 46, 58]. These references all worked in the chiral limit, and the transformation used there was defined by $g_R = \mathbb{1}$ and $g_L = \Sigma_0^\dagger$. In the chiral limit, the pion condensate is maximal, $\cos\theta = 0$, for all μ_I, as can be seen for instance from Eq. (7) (as we shall see later, this is true even in the presence of baryons). In this case, this alternative transformation gives the identity in the right-handed sector and $g_L\tau_3 g_L^\dagger = -\tau_3$ for all α (with a rotation in the τ_1-τ_2 sector that depends on α) in the left-handed sector. Hence, this choice is particularly simple. However, generalizing this transformation to the case of a non-zero pion mass leads to asymmetric values in left- and right-handed sectors. This is avoided by the symmetric choice (10), which will allow us to work with symmetric or antisymmetric boundary conditions for any value of θ.

2.2 Holographic setup including effective mass term

The WSS model [6–8] is a top-down string-theoretical construction describing the near-horizon geometry of a non-supersymmetric configuration sourced by N_c D4-branes. The

flavor sector is included by adding N_f D8-$\overline{\text{D8}}$-brane pairs which we assume to be maximally separated along a compact circle $X_4 \sim X_4 + 2\pi M_{\rm KK}^{-1}$. The flavor branes thus follow geodesics, hence their embedding does not have to be determined dynamically. In the so-called confined geometry, the induced metric on the flavor branes takes the form

$$ds^2 = \left(\frac{U}{R}\right)^{3/2}\left(dX_0^2 + d\boldsymbol{X}^2\right) + \left(\frac{R}{U}\right)^{3/2}\left[\frac{dU^2}{f(U)} + U^2 d\Omega_4^2\right], \qquad f(U) = 1 - \frac{U_{\rm KK}^3}{U^3}\,. \quad (13)$$

Here, U is the coordinate for the radial holographic direction, $d\Omega_4^2$ describes the unit 4-sphere, R is the background curvature radius, which is related to the string length ℓ_s, the 't Hooft coupling and the Kaluza-Klein mass via $R^3 = \lambda\ell_s^2/(2M_{\rm KK})$, and $U_{\rm KK} = 2\lambda M_{\rm KK}\ell_s^2/9$ is the location where the X_4 direction caps off. Four-dimensional Euclidean space-time is given by $(X_0, \boldsymbol{X})$, where the temporal component $X_0 \sim X_0 + T^{-1}$ is compact in the presence of a non-zero temperature T. In this version of the model, large N_c effects render the flavor physics temperature independent, so that T will appear only as an overall factor in the free energy.

The action on the flavor branes is composed of the Dirac-Born-Infeld (DBI) and Chern-Simons (CS) contributions, together with our effective mass term,

$$S = S_{\rm DBI} + S_{\rm CS} + S_{\rm m}\,. \quad (14)$$

We now discuss each of these terms separately.

2.2.1 Yang-Mills and Chern-Simons contributions

The DBI action is

$$S_{\rm DBI} = 2T_8 V_4 \int d^4X \int_{U_{\rm KK}}^{\infty} dU e^{-\phi}\,{\rm STr}\sqrt{\det(g + 2\pi\alpha'\mathcal{F})}\,, \quad (15)$$

where $T_8 = 1/\left[(2\pi)^8\ell_s^9\right]$ is the D8-brane tension, $V_4 = 8\pi^2/3$ is the volume of the 4-sphere, $e^{\phi} = g_s(U/R)^{3/4}$ is the dilaton with the string coupling $g_s = \lambda/(2\pi N_c M_{\rm KK}\ell_s)$, and $\alpha' = \ell_s^2$. The prefactor 2 accounts for the two halves of the connected flavor branes. The metric g is given by Eq. (13), and the field strength $\mathcal{F}$ can be expressed in terms of the world-volume gauge field $\mathcal{A}$ as

$$\mathcal{F}_{\mu\nu} = \partial_\mu\mathcal{A}_\nu - \partial_\nu\mathcal{A}_\mu + i[\mathcal{A}_\mu, \mathcal{A}_\nu]\,, \quad (16)$$

with $\mu, \nu \in \{0, 1, 2, 3, U\}$. We work with $N_f = 2$, and, following the convention of Ref. [39], introduce the dimensionless coordinates

$$u = \frac{U}{R(M_{\rm KK}R)^2}\,, \qquad x_0 = \lambda_0 M_{\rm KK}X_0\,, \qquad x_i = M_{\rm KK}X_i\,, \quad (17)$$

where $i = 1, 2, 3$, and where we have abbreviated

$$\lambda_0 \equiv \frac{\lambda}{4\pi}\,. \quad (18)$$

In these dimensionless units,

$$u_{\rm KK} = \frac{4}{9}\,. \quad (19)$$

The corresponding dimensionless gauge fields, decomposed into $U(1)$ and $SU(2)$ parts, are introduced via

$$\mathcal{A}_U = \frac{\hat{A}_u + A_u^a\tau_a}{R(M_{\rm KK}R)^2}\,, \qquad \frac{\mathcal{A}_0}{\lambda_0 M_{\rm KK}} = \hat{A}_0 + A_0^a\tau_a\,, \qquad \frac{\mathcal{A}_i}{M_{\rm KK}} = \hat{A}_i + A_i^a\tau_a\,. \quad (20)$$

Accordingly, we introduce abelian and non-abelian components of the dimensionless field strengths

$$F_{\mu\nu} = \hat{F}_{\mu\nu} + F^a_{\mu\nu}\tau_a \,, \tag{21}$$

with

$$\hat{F}_{\mu\nu} = \partial_\mu \hat{A}_\nu - \partial_\nu \hat{A}_\mu \,, \qquad F^a_{\mu\nu} = \partial_\mu A^a_\nu - \partial_\nu A^a_\mu - 2\epsilon_{abc} A^b_\mu A^c_\nu \,. \tag{22}$$

Moreover, we shall from now on assume all fields to be independent of Euclidean space-time, i.e., they only depend on the holographic coordinate u. Then, the space-time integration becomes trivial and simply yields a prefactor V/T, where V is the 3-volume of our system. We work with the Yang-Mills (YM) approximation to the DBI action, keeping only terms of second order in the field strength. In this approximation, there is no ambiguity in calculating the action, the symmetrized trace in Eq. (15) is identical to an ordinary trace. The result is

$$\begin{aligned} S_{\rm DBI} \simeq S_{\rm YM} &= \frac{\mathcal{N}}{2}\frac{V}{T}\int_{u_{\rm KK}}^{\infty} du \left[u^{5/2}\sqrt{f}\left(\mathrm{Tr}[F^2_{0u}] + \frac{\mathrm{Tr}[F^2_{iu}]}{\lambda_0^2}\right)\right. \\ &\left. + \frac{1}{u^{1/2}\sqrt{f}}\left(\mathrm{Tr}[F^2_{0i}] + \frac{\mathrm{Tr}[F^2_{ij}]}{2\lambda_0^2}\right)\right] , \end{aligned} \tag{23}$$

where we have abbreviated

$$\mathcal{N} = \frac{N_c M_{\rm KK}^4 \lambda_0^3}{6\pi^2} \,. \tag{24}$$

The CS action can be written in terms of abelian and non-abelian components as [23, 58]

$$\begin{aligned} S_{\rm CS} &= -i\frac{\mathcal{N}}{2\lambda_0^2}\frac{V}{T}\int_{u_{\rm KK}}^{\infty} du \left\{ \frac{3}{2}\hat{A}_\mu\left(F^a_{\nu\rho}F^a_{\sigma\lambda} + \frac{1}{3}\hat{F}_{\nu\rho}\hat{F}_{\sigma\lambda}\right)\right. \\ &\left. + 2\partial_\mu\left[\hat{A}_\nu\left(F^a_{\rho\sigma}A^a_\lambda + \frac{1}{4}\epsilon_{abc}A^a_\rho A^b_\sigma A^c_\lambda\right)\right]\right\}\epsilon^{\mu\nu\rho\sigma\lambda} \,. \end{aligned} \tag{25}$$

In all situations we consider in this paper, the non-zero field strengths are the abelian and non-abelian temporal components $\hat{A}_0(u)$, $A^a_0(u)$ (needed to account for the chemical potentials) and the non-abelian spatial components $A^a_i(u)$ (accounting for baryonic matter and rho meson condensation). In particular, we will always work in a gauge where $\hat{A}_u = A^a_u = 0$, in which case the pion field is encoded in the boundary conditions for $A^a_0(u)$ [7]. We denote

$$\hat{A}_0(u) \equiv iA(u) \,, \qquad A^a_0(u) \equiv iK_a(u) \,, \tag{26}$$

where the factor i is due to the Euclidean signature of space-time, and where the simplified notation of the temporal gauge fields is introduced to avoid cluttering of indices, in particular in Sec. 3. Then, the YM and CS contributions to the action become

$$S_{\rm YM} + S_{\rm CS} = N_f \mathcal{N}\frac{V}{T}\int_{u_{\rm KK}}^{\infty} du\, \mathcal{L} \,, \tag{27}$$

with the dimensionless Lagrangian

$$\begin{aligned} \mathcal{L} &= \frac{u^{5/2}\sqrt{f}}{2}\left(-A'^2 - K'_aK'_a + \frac{A^{a\prime}_i A^{a\prime}_i}{\lambda_0^2}\right) + \frac{2}{u^{1/2}\sqrt{f}}\left[-K_aK_aA^b_iA^b_i + K_aK_bA^a_iA^b_i\right. \\ &\left. + \frac{A^a_iA^a_iA^b_jA^b_j - A^a_iA^a_jA^b_iA^b_j}{2\lambda_0^2}\right] + \frac{A}{\lambda_0^2}\epsilon_{ijk}\epsilon_{abc}(A^a_iA^b_jA^c_k)' \,, \end{aligned} \tag{28}$$

where the last term comes from the CS contribution (only the first term in Eq. (25) contributes), and where prime denotes derivative with respect to u. The resulting equations of motion are

$$(u^{5/2}\sqrt{f}A')' = -\frac{1}{\lambda_0^2}\epsilon_{ijk}\epsilon_{abc}(A_i^a A_j^b A_k^c)' , \tag{29a}$$

$$(u^{5/2}\sqrt{f}K_a')' = \frac{4}{u^{1/2}\sqrt{f}}(K_a A_i^b A_i^b - K_b A_i^b A_i^a) , \tag{29b}$$

$$(u^{5/2}\sqrt{f}A_i^{a\prime})' = \frac{4\lambda_0^2}{u^{1/2}\sqrt{f}}\left(-K_b K_b A_i^a + K_a K_b A_i^b + \frac{A_i^a A_j^b A_j^b - A_j^a A_i^b A_j^b}{\lambda_0^2}\right)$$
$$-3A'\epsilon_{ijk}\epsilon_{abc}A_j^b A_k^c . \tag{29c}$$

2.2.2 Mass correction

Finally, we need to specify the effective mass term in the action $S_{\rm m}$. The WSS model differs from other holographic constructions in that the inclusion of the pion mass cannot be described directly in terms of a separation of the flavor branes from the color branes in a transverse direction. Here we follow the approach of Refs. [42–44], see also Refs. [36, 45, 68–70], where the pion mass is included in an effective way by considering an open Wilson line stretched between the D8- and $\overline{\rm D8}$-branes. Its expectation value is given by the corresponding worldsheet action, $\langle\mathcal{O}\rangle = ce^{-S_{\rm WS}}$ with a constant c and $S_{\rm WS} = S_{\rm NG} + S_\partial$, and one identifies the (medium dependent) chiral condensate with $\langle\bar{q}q\rangle = -ce^{-S_{\rm NG}}$. The Nambu-Goto action takes the form

$$S_{\rm NG} = 2\lambda_0\int_{u_{\rm KK}}^{\infty} du\, x_4(u) , \tag{30}$$

with $x_4 = M_{\rm KK}X_4$, in analogy to the spatial coordinates x_i (17). Since we work with maximally separated flavor branes, the embedding function is constant, $x_4 = \pi/2$, and thus $S_{\rm NG}$ merely contains a constant (infinite) vacuum contribution. Subtracting this vacuum contribution, the factor from the Nambu-Goto action is 1. This is in contrast to the case of non-antipodal separation of the flavor branes, where the embedding is medium-dependent and the Nambu-Goto factor gives a non-trivial contribution to the equations of motion [36, 45]. The boundary term S_∂ is given by

$$e^{-S_\partial} = \exp\left(i\int_{-\infty}^{\infty} dZ\,\mathcal{A}_Z\right) \equiv \Sigma . \tag{31}$$

Here we have introduced the new radial coordinate via

$$u^3 = u_{\rm KK}^3 + u_{\rm KK}z^2 , \tag{32}$$

and the dimensionful version Z is obtained from z in the same way as U is obtained from u (17). The coordinate $z \in [-\infty, \infty]$ runs from the ultraviolet boundary of the D8-branes to that of the $\overline{\rm D8}$-branes, with $z = 0$ being at the tip of the connected branes at $u = u_{\rm KK}$. We will often switch between the coordinates u and z according to which one is more convenient for a given calculation or argument, and when we integrate over $u \in [u_{\rm KK}, \infty]$ we assume that we are on the $z > 0$ half of the connected branes. The holonomy (31) can be identified with the chiral field Σ introduced in the previous subsection in the context of chiral perturbation theory [7]. Therefore, by choosing $c = f_\pi^2 B$, the contribution to the

action from the open Wilson line can be matched to the lowest-order mass term of chiral perturbation theory, such that

$$S_{\rm m} = -\frac{V}{T}\frac{f_\pi^2 B}{2}{\rm Tr}[M\Sigma^\dagger + M^\dagger\Sigma]\,, \tag{33}$$

where we have already assumed our system to be homogeneous. With the chiral field $\Sigma = \Sigma_0$ (8) and using the result for the pion decay constant in terms of the parameters of the WSS model [7]

$$f_\pi^2 = \frac{2N_c M_{\rm KK}^2\lambda_0}{27\pi^3}\,, \tag{34}$$

the contribution to the action (33) reduces to

$$S_{\rm m} = -\frac{V}{T}\mathcal{N}N_f\frac{2\bar{m}_\pi^2\cos\theta}{9\pi}\,, \tag{35}$$

where we have introduced the dimensionless pion mass

$$\bar{m}_\pi \equiv \frac{m_\pi}{\lambda_0 M_{\rm KK}}\,. \tag{36}$$

Since the trace is invariant under chiral transformations, the result (35) is independent of whether the rotation (12) is performed on Σ_0 and M or not. Therefore, the result is also valid for $\mathcal{A}_Z = 0$, for which the chiral field (31) is trivial, but the condensate sits in the rotated matrix M'. Within our setup the effective mass term does not contain any gauge field and thus the equations of motion (29) remain unaltered. However, $S_{\rm m}$ is not a mere constant since it contains the charged pion condensate θ with respect to which we need to minimize the free energy and which enters the gauge fields through the boundary conditions, as we will discuss below. We also note that the identification with the chiral field (31) only works if there is no additional contribution to the holonomy from baryons. We shall comment on this possibility in more detail below Eq. (51).

We can now put together all pieces of our action, Eqs. (27) and (35), to obtain

$$S = \mathcal{N}N_f\frac{V}{T}\left[\int_{u_{\rm KK}}^\infty du\,\mathcal{L} - \frac{2\bar{m}_\pi^2}{9\pi}(\cos\theta - 1)\right]\,, \tag{37}$$

with the Lagrangian (28). In the vacuum, all gauge fields vanish and thus YM and CS contributions are zero, while the mass term (35) yields a vacuum contribution for $\theta = 0$, which we have subtracted in Eq. (37) to normalize the vacuum pressure to zero.

The grand-canonical potential (= free energy density) is obtained from the on-shell action,

$$\Omega = \frac{T}{V}S\Big|_{\rm on-shell}\,, \tag{38}$$

and we shall later work with the dimensionless version

$$\bar{\Omega} = \frac{\Omega}{\mathcal{N}N_f} = \int_{u_{\rm KK}}^\infty du\,\mathcal{L} - \frac{2\bar{m}_\pi^2}{9\pi}(\cos\theta - 1)\,. \tag{39}$$

2.3 Reproducing chiral perturbation theory in the WSS model

The action set up in the previous subsection will be used for our main results, where we account for meson condensation and baryonic matter. First, in this subsection, we explain how the results of lowest-order chiral perturbation theory from Sec. 2.1 are reproduced. This will be useful to understand the more complicated calculation in Sec. 3.

In the purely mesonic case it is consistent to set all gauge fields to zero except for the non-abelian temporal components K_a. The CS term does not contribute in this scenario, and the Lagrangian (28) reduces to

$$\mathcal{L} = -\frac{u^{5/2}\sqrt{f}}{2} K'_a K'_a \,. \tag{40}$$

The only non-trivial equation of motion (29b) is

$$\partial_u (u^{5/2}\sqrt{f} K'_a) = 0 \,. \tag{41}$$

In terms of the coordinate z (32) this yields the solutions

$$K_a(z) = C_a + D_a \arctan \frac{z}{u_{\rm KK}} \,, \tag{42}$$

with integration constants C_a, D_a. According to the usual dictionary of the gauge/gravity correspondence, the boundary value of the temporal component of the gauge field corresponds to the chemical potential of the field theory. The isospin chemical potential corresponds, in the unrotated basis, to the boundary value of the third component K_3. More precisely, we work with a vector isospin chemical potential, whose value is the same in the left- and right-handed sectors such that[2] $K_3(z = \pm\infty) = \bar{\mu}_I/2$. Here and in the following we work with dimensionless chemical potentials according to the dimensionless gauge fields of Eq. (20), i.e., we define[3]

$$\bar{\mu}_B = \frac{\mu_B}{\lambda_0 N_c M_{\rm KK}} \,, \qquad \bar{\mu}_I = \frac{\mu_I}{\lambda_0 M_{\rm KK}} \,. \tag{43}$$

Since we have made the gauge choice $\mathcal{A}_Z = 0$, our chiral field (31) is trivial and it appears we cannot describe pion condensation. This problem can be circumvented by applying the chiral rotation (9), by which we effectively move the pion condensate from the chiral field into the boundary conditions for K_a [39, 46, 58]. In the massless case, the rotation applied in Refs. [39, 46, 58] simply flips the sign of the boundary condition for K_3 on the left-handed boundary, and one can easily solve the system with $K_1(z) = K_2(z) = 0$. Since we work with a non-zero pion mass, it is more convenient to apply the rotation (12), as already explained below that equation. This yields the boundary conditions

$$K_1(z \to \pm\infty) = \mp \frac{\bar{\mu}_I}{2} \sin\theta \sin\alpha \,, \tag{44a}$$

$$K_2(z \to \pm\infty) = \pm \frac{\bar{\mu}_I}{2} \sin\theta \cos\alpha \,, \tag{44b}$$

$$K_3(z \to \pm\infty) = \frac{\bar{\mu}_I}{2} \cos\theta \,. \tag{44c}$$

We see that in general all three gauge field components become nonzero. With these

[2] This convention for μ_I matches the one of Sec. 2.1, where the onset of pion condensation is at $\mu_I = m_\pi$, but it differs from our previous holographic study [39] by a factor 2.

[3] The factor N_c in the baryon chemical potential is included because the boundary value of the gauge field corresponds to the *quark* chemical potential, whose dimensionless version, following the notation of Ref. [40], we denote by $\bar{\mu}_B$. This ensures that μ_B as used in all our physical results is the actual *baryon* chemical potential, which differs by a factor N_c from the quark chemical potential.

boundary conditions the solutions (42) become

$$K_1(z) = -\frac{\bar{\mu}_I}{\pi}\sin\theta\sin\alpha\arctan\frac{z}{u_{\rm KK}}\,, \tag{45a}$$

$$K_2(z) = \frac{\bar{\mu}_I}{\pi}\sin\theta\cos\alpha\arctan\frac{z}{u_{\rm KK}}\,, \tag{45b}$$

$$K_3(z) = \frac{\bar{\mu}_I}{2}\cos\theta\,. \tag{45c}$$

Inserting these solutions into the free energy (38), one finds that the free energy density is identical to the one from chiral perturbation theory, Eq. (6) with $\psi = 0$. The dimensionless free energy (39) becomes

$$\bar{\Omega} = -\frac{3u_{\rm KK}^{3/2}\bar{\mu}_I^2\sin^2\theta}{8\pi} - \frac{2\bar{m}_\pi^2}{9\pi}(\cos\theta - 1)\,. \tag{46}$$

After minimizing with respect to θ, the equivalent of Eq. (7) for pion condensate, free energy density, and isospin density in terms of the dimensionless quantities of the holographic calculation is

$$\cos\theta = \frac{\bar{m}_\pi^2}{\bar{\mu}_I^2}\,, \qquad \bar{\Omega} = -\frac{\bar{\mu}_I^2}{9\pi}\left(1 - \frac{\bar{m}_\pi^2}{\bar{\mu}_I^2}\right)^2\,, \qquad \bar{n}_I = -\frac{\partial\bar{\Omega}}{\partial\bar{\mu}_I} = \frac{2\bar{\mu}_I}{9\pi}\left(1 - \frac{\bar{m}_\pi^4}{\bar{\mu}_I^4}\right)\,, \tag{47}$$

where we have used Eq. (19). The dimensionless isospin density $\bar{n}_I$ – and, for completeness and later use, baryon density $\bar{n}_B$ – are related to their dimensionful counterparts n_I, n_B by

$$n_{B,I} = \frac{N_f\lambda_0^2 M_{\rm KK}^3}{6\pi^2}\bar{n}_{B,I}\,. \tag{48}$$

3 Adding baryons

In this section we introduce baryonic degrees of freedom and explain the setup used for our main results. Baryons in the WSS model are understood as instantonic configurations of the worldvolume gauge fields, such that baryon and instanton numbers are identified. Near the tip of the flavor branes at $z = 0$ a (static) single baryon is well approximated by the classical Belavin-Polyakov-Schwartz-Tyupkin (BPST) configuration [71], where spatial directions are locked to the internal $SU(2)$ directions, $A_i \propto \tau_i$. One can then quantize the collective coordinates [72] in order to identify baryonic states with different spin, isospin, and excitation numbers. This procedure was used to compute static properties of the holographic baryonic states [23].

For many-baryon systems the instantonic picture becomes complicated and it is useful to resort to a simpler approximation. Here we follow Refs. [30,32] and consider a spatially homogeneous distribution of baryonic matter. This can be thought of as highly overlapping instantons and thus we expect this approximation to be accurate at sufficiently large baryon densities. Although it captures part of the relevant physics, the classical treatment of isospin-asymmetric matter we shall employ here induces some unrealistic (large-N_c) artifacts. Most notably, it leads to a symmetry energy much larger than in the real world [39]. It was recently proposed to re-introduce the collective coordinate quantization at the level of the homogeneous ansatz to (partially) remedy this deficiency [57]. Here we do not attempt to combine this quantization with our improved ansatz but emphasize that this is a promising idea for future studies.

3.1 Improved ansatz for isospin-asymmetric baryonic matter

Our ansatz for the spatial components of the non-abelian gauge fields is (no summation over i)

$$A_i^a(u) = -\frac{\lambda_0}{2} h_i(u) \delta_i^a \,, \tag{49}$$

where the functions $h_i(u)$ have to be determined dynamically.

This ansatz deserves a few comments. We first observe that, in general, it is *not* consistent to omit all off-diagonal gauge fields $a \neq i$. This can be seen from Eq. (29c): if off-diagonal gauge fields are set to zero on the right-hand side of this equation, its second term survives and gives a contribution of the form $K_a K_i h_i$ (no summation over i). If this contribution is non-zero, the corresponding A_i^a must be non-trivial (and, in turn, more non-zero terms on the right-hand side are generated). Obviously, if all spatial gauge field components vanish, including the functions h_i, there is no inconsistency. This is what we did in the previous section.

There are two more situations in which the off-diagonal components can be switched off consistently, while keeping the diagonal components non-vanishing.

(i) *isotropic limit:* for $\mu_I = 0$ all functions $K_i(u)$ vanish and a consistent solution exists for $h_1 = h_2 = h_3$. This approximation was extrapolated to non-zero μ_I (where it is no longer a solution to the equations of motion) in Ref. [39].

(ii) *chiral limit:* in the limit of vanishing pion mass the pion condensate is always maximal, $\sin\theta = 1$, and thus the global rotation employed in Refs. [39,46,58] only affects the τ_3 component and the isospin chemical potential does not generate non-zero boundary conditions for K_1 and K_2. Therefore, these two components can be set to zero such that $K_a K_i h_i = 0$ for all $a \neq i$ even in the presence of non-zero functions $h_i(u)$.

Here, we are interested in the entire μ_B-μ_I phase diagram, including a physical pion mass and anisotropic solutions. Therefore, strictly speaking, we need to account for off-diagonal gauge components as well, which leads to a very complicated system of equations. It seems we are in trouble. Our solution to this problem is to work with the ansatz (49) as an approximation. The idea is that this ansatz captures the two limits (i) and (ii) correctly in the regimes where they are valid, while it provides an interpolation for the region in between. We will make this more explicit in Sec. 5.2 with the help of the numerical solutions, showing that the in-between region is in fact very rigidly constrained by the two limits. The benefit is that we can work with a more manageable system of equations for which no further approximation is needed; in particular, all remaining variables, including the infrared boundary values for the functions h_i, can be determined fully dynamically.

With the ansatz (49), the Lagrangian (28) can be written as

$$\mathcal{L} = \frac{u^{5/2}}{2\sqrt{f}} (g_1 - f A'^2 - f K_a' K_a' + g_2 - g_3) - \frac{3\lambda_0}{4} A (h_1 h_2 h_3)' \,, \tag{50}$$

where, generalizing the notation of Ref. [39] to three different functions $h_i(u)$, we have abbreviated

$$g_1 \equiv \frac{f}{4}(h_1'^2 + h_2'^2 + h_3'^2) \,, \tag{51a}$$

$$g_2 \equiv \frac{\lambda_0^2}{4u^3}(h_1^2 h_2^2 + h_1^2 h_3^2 + h_2^2 h_3^2) \,, \tag{51b}$$

$$g_3 \equiv \frac{\lambda_0^2}{u^3}\left[K_1^2(h_2^2 + h_3^2) + K_2^2(h_1^2 + h_3^2) + K_3^2(h_1^2 + h_2^2)\right] \,. \tag{51c}$$

The action is still given by Eq. (37) with no further contributions from baryons. In particular, the effective mass term is the same as in the purely mesonic case. The reason is that in our homogeneous ansatz we have $\mathcal{A}_Z = 0$, and thus there is no baryonic contribution to the boundary term (31). This is different in the instantonic picture. In this case, even for a single instanton, the boundary term gives a contribution, which is a correction to the baryon mass from non-zero bare quark masses [69]. Generalizing this calculation to a non-interacting instanton gas would give a correction to our action proportional to $m_\pi n_B$. However, our homogeneous ansatz does not know about the mass of single baryons and thus this contribution is absent. This is also plausible from a physical point of view since we expect this mass correction to be small for large chemical potentials (the $m_\pi n_B$ contribution to the free energy being small compared to terms of order $\mu_B n_B$), and this regime is exactly the one where our homogeneous ansatz is valid.

For a given configuration, the baryon number density is computed from the topological instanton number,

$$n_B = \frac{\lambda_0^3 M_{\mathrm{KK}}^3}{8\pi^2} \int_{-\infty}^{\infty} dz\, \partial_z (h_1 h_2 h_3)\,. \tag{52}$$

Therefore, n_B is only non-zero if the product $h_1 h_2 h_3$ is discontinuous somewhere in the bulk. We assume the discontinuity to sit at $z = 0$ and denote the values of the functions $h_i(z)$ at this point by

$$h_{ic}^{\pm} \equiv h_i(z \to 0^{\pm})\,. \tag{53}$$

It is conceivable that an instanton system splits into two or more layers in the z direction as the density is increased [31, 33, 34, 36, 73], which would correspond to our discontinuity in $h_1 h_2 h_3$ moving up in z with its location determined dynamically (and possibly more than one discontinuity appearing). For simplicity we will ignore this possibility in the following.

Our choice for the rotation (10) allows us to work only with functions which are either symmetric or antisymmetric under $z \to -z$, hence we can write

$$h_{ic}^{-} = e_i h_{ic}^{+}\,, \tag{54}$$

where $e_i \in \{-1, 1\}$. With the definition of the dimensionless baryon density (48), we thus obtain from Eq. (52)

$$\bar{n}_B = -\frac{3\lambda_0}{4} h_{1c} h_{2c} h_{3c}\,, \tag{55}$$

where we have already used $e_1 e_2 e_3 = -1$ as a requirement for a non-zero baryon density, and have denoted $h_{ic} \equiv h_{ic}^{+}$ for notational convenience.

As for a single instanton, we require the spatial components of the gauge field to vanish in the ultraviolet,

$$h_i(z \to \pm\infty) = 0\,. \tag{56}$$

The ultraviolet boundary condition of the temporal component of the abelian gauge field is given by the baryon chemical potential,

$$A(z \to \pm\infty) = \bar{\mu}_B\,, \tag{57}$$

while for the non-abelian temporal components $K_a(z)$ we require Eq. (44).

Due to the symmetry of our system we do not expect baryonic matter to be asymmetric in the $\tau_{1,2}$ directions. Hence, we may set

$$h_1(u) = h_2(u) \equiv h(u)\,. \tag{58}$$

(And, consequently, we denote $h_c \equiv h_{1c} = h_{2c}$.) A non-zero baryon density is now only achieved for $e_3 = -1$ and thus in this case $h_3(z)$ is anti-symmetric in z and discontinuous while $h(z)$ can be either symmetric (and thus continuous) or anti-symmetric.

3.2 Equations of motion, free energy and minimization conditions

Within this ansatz, the equation of motion for the abelian gauge field (29a) reduces to

$$(u^{5/2}\sqrt{f}A')' = \frac{3\lambda_0}{4}(h^2 h_3)' \,, \tag{59}$$

which is easily integrated to give

$$A'(u) = \frac{\bar{n}_B Q(u)}{u^{5/2}\sqrt{f(u)}} \,, \qquad Q(u) \equiv 1 - \frac{h^2(u)h_3(u)}{h_c^2 h_{3c}} \,. \tag{60}$$

For the temporal components of the non-abelian gauge potentials we find from Eq. (29b)

$$(u^{5/2}\sqrt{f}K_1')' = \frac{\lambda_0^2 K_1(h^2+h_3^2)}{u^{1/2}\sqrt{f}} \,, \tag{61a}$$

$$(u^{5/2}\sqrt{f}K_2')' = \frac{\lambda_0^2 K_2(h^2+h_3^2)}{u^{1/2}\sqrt{f}} \,, \tag{61b}$$

$$(u^{5/2}\sqrt{f}K_3')' = \frac{2\lambda_0^2 K_3 h^2}{u^{1/2}\sqrt{f}} \,. \tag{61c}$$

Finally, the equations of motion for the spatial components of the gauge fields (29c) become

$$(u^{5/2}\sqrt{f}h')' - \frac{3\lambda_0 h h_3 \bar{n}_B Q}{u^{5/2}\sqrt{f}} = \frac{\lambda_0^2 h}{u^{1/2}\sqrt{f}}\left(h^2+h_3^2-2K_1^2-2K_2^2-4K_3^2\right) \,, \tag{62a}$$

$$(u^{5/2}\sqrt{f}h_3')' - \frac{3\lambda_0 h^2 \bar{n}_B Q}{u^{5/2}\sqrt{f}} = \frac{\lambda_0^2 h_3}{u^{1/2}\sqrt{f}}\left(2h^2-4K_1^2-4K_2^2\right) \,, \tag{62b}$$

where we have already inserted the solution for A (60).

Equations (61) and (62) can obviously not be integrated as easily as Eq. (59) and will have to be solved numerically. Simultaneously, we will need to determine the charged pion condensate θ and the boundary values h_c, h_{3c} by minimizing the free energy. To this end, we take the derivative of the free energy with respect to a generic variable $x \in \{\theta, h_c, h_{3c}, \bar{\mu}_B, \bar{\mu}_I, \alpha\}$, with all other variables in this set kept fixed. Here we have included the chemical potentials in order to derive an expression for the isospin density $\bar{n}_I$ and to confirm the usual thermodynamic relation between the free energy and the baryon number density $\bar{n}_B$. We have also included the angle α to verify as a consistency check that the free energy does not depend on this angle. From Eq. (39) and $\mathcal{L} = \mathcal{L}(A, K_a, h, h_3; A', K_a', h', h_3')$ we compute

$$\begin{aligned}\frac{\partial\bar{\Omega}}{\partial x} = \frac{1}{2}\int_{-\infty}^{\infty} dz \Bigg[&-\partial_z\left(u^{5/2}\sqrt{f}A'\frac{\partial A}{\partial x}\right) + \partial_z\left(\frac{u^{5/2}\sqrt{f}h' - 3\lambda_0 A h h_3}{2}\frac{\partial h}{\partial x}\right) \\ &-\partial_z\left(u^{5/2}\sqrt{f}K_i'\frac{\partial K_i}{\partial x}\right) + \partial_z\left(\frac{u^{5/2}\sqrt{f}h_3' - 3\lambda_0 A h^2}{4}\frac{\partial h_3}{\partial x}\right)\Bigg] + \frac{2\bar{m}_\pi^2 \sin\theta}{9\pi}\frac{\partial\theta}{\partial x} \,,\end{aligned} \tag{63}$$

where we have used the equations of motion. The various terms on the right-hand side can receive contributions from the ultraviolet boundary but also from the infrared discontinuities at $z = 0$ ($u = u_{\rm KK}$). The gauge potentials $A(z)$, $K_a(z)$ are taken to be continuous

and smooth across $z = 0$. The boundary condition (57) dictates that $A(z)$ is even in z, and its behavior near $u = u_{\rm KK}$ is

$$A(u) = A_c + \mathcal{O}(u - u_{\rm KK})\,, \tag{64}$$

with A_c to be determined dynamically. Due to the boundary conditions (44), $K_1(z)$ and $K_2(z)$ are odd, while $K_3(z)$ is even, and their infrared behavior is

$$K_1(u) = K_{1(1)}\sqrt{u - u_{\rm KK}} + \ldots = \frac{K_{1(1)}}{\sqrt{3u_{\rm KK}}}\, z + \ldots\,, \tag{65a}$$

$$K_2(u) = K_{2(1)}\sqrt{u - u_{\rm KK}} + \ldots = \frac{K_{2(1)}}{\sqrt{3u_{\rm KK}}}\, z + \ldots\,, \tag{65b}$$

$$K_3(u) = K_{3c} + \mathcal{O}(u - u_{\rm KK})\,, \tag{65c}$$

with the slopes $K_{1(1)}$ and $K_{2(1)}$ and the boundary value K_{3c} to be determined dynamically. As discussed above, the functions h and h_3 can (and for $\bar{n}_B \neq 0$ at least h_3 must) have a discontinuity at $z = 0$. Their infrared behavior is

$$h(u) = h_c + h_{(1)}\sqrt{u - u_{\rm KK}} + \ldots = h_c + \frac{h_{(1)}}{\sqrt{3u_{\rm KK}}}\, z + \ldots\,, \tag{66a}$$

$$h_3(u) = h_{3c} + h_{3(1)}\sqrt{u - u_{\rm KK}} + \ldots = h_{3c} + \frac{h_{3(1)}}{\sqrt{3u_{\rm KK}}}\, z + \ldots\,. \tag{66b}$$

Here, $h_c, h_{3c}, h_{(1)}, h_{3(1)}$ are all a priori unknown.

We can now go back to Eq. (63) to compute

$$\begin{aligned}\frac{\partial\bar{\Omega}}{\partial x} &= -\bar{n}_B\frac{\partial\bar{\mu}_B}{\partial x} + \frac{1}{2}\frac{\partial\bar{\mu}_I}{\partial x}\left(\kappa_1\sin\theta\sin\alpha - \kappa_2\sin\theta\cos\alpha - \kappa_3\cos\theta\right) + \frac{2\bar{m}_\pi^2\sin\theta}{9\pi}\frac{\partial\theta}{\partial x}\\ &+\frac{\bar{\mu}_I}{2}\frac{\partial\theta}{\partial x}\left(\kappa_1\cos\theta\sin\alpha - \kappa_2\cos\theta\cos\alpha + \kappa_3\sin\theta\right) + \frac{\bar{\mu}_I\sin\theta}{2}\frac{\partial\alpha}{\partial x}\left(\kappa_1\cos\alpha + \kappa_2\sin\alpha\right)\\ &+\frac{1}{4}\frac{\partial h_c}{\partial x}\left(-\sqrt{3}u_{\rm KK}^2 h_{(1)} + 6\lambda_0 A_c h_c h_{3c}\right) + \frac{1}{8}\frac{\partial h_{3c}}{\partial x}\left(-\sqrt{3}u_{\rm KK}^2 h_{3(1)} + 6\lambda_0 A_c h_c^2\right)\,.\end{aligned} \tag{67}$$

This result is derived independent of whether h is continuous or not, but does assume its derivative to be discontinuous. In other words, $h(z)$ is odd and discontinuous or even and continuous but with a cusp. We have abbreviated

$$\kappa_i \equiv (u^{5/2}\sqrt{f}K_i')_{u=\infty}\,, \tag{68}$$

which, using the equations of motion (61) and the expansions (65), can be expressed as

$$\kappa_1 = \frac{\sqrt{3}u_{\rm KK}^2}{2}K_{1(1)} + \lambda_0^2\int_{u_{\rm KK}}^\infty du\,\frac{K_1(h^2+h_3^2)}{u^{1/2}\sqrt{f}}\,, \tag{69a}$$

$$\kappa_2 = \frac{\sqrt{3}u_{\rm KK}^2}{2}K_{2(1)} + \lambda_0^2\int_{u_{\rm KK}}^\infty du\,\frac{K_2(h^2+h_3^2)}{u^{1/2}\sqrt{f}}\,, \tag{69b}$$

$$\kappa_3 = 2\lambda_0^2\int_{u_{\rm KK}}^\infty du\,\frac{K_3 h^2}{u^{1/2}\sqrt{f}}\,. \tag{69c}$$

From Eq. (67) we can easily read off the derivatives with respect to all possible values of x. Let us start with $x = \alpha$, in which case we expect the derivative to vanish. We see that it vanishes trivially in the absence of a charged pion condensate, $\theta = 0$. If θ is non-zero, we use the following observation to show that the derivative is still zero. With partial integration and using the equation of motion for K_1 (61a) we have

$$\int_{u_{\rm KK}}^{\infty} du\, u^{5/2}\sqrt{f}K_1'K_2' = \kappa_1\frac{\bar{\mu}_I}{2}\sin\theta\cos\alpha - \lambda_0^2\int_{u_{\rm KK}}^{\infty} du\,\frac{K_1K_2(h^2+h_3^2)}{u^{1/2}\sqrt{f}}\,, \tag{70}$$

and, on the other hand, by exchanging the roles of K_1 and K_2 in the partial integration we get the alternative expression for the same integral

$$\int_{u_{\rm KK}}^{\infty} du\, u^{5/2}\sqrt{f}K_1'K_2' = -\kappa_2\frac{\bar{\mu}_I}{2}\sin\theta\sin\alpha - \lambda_0^2\int_{u_{\rm KK}}^{\infty} du\,\frac{K_1K_2(h^2+h_3^2)}{u^{1/2}\sqrt{f}}\,. \tag{71}$$

Subtracting Eq. (71) from Eq. (70) gives $\kappa_1\cos\alpha + \kappa_2\sin\alpha = 0$, and thus the free energy does indeed not depend on α.

Next, we turn to the thermodynamic relations for baryon and isospin densities by choosing $x \in \{\bar{\mu}_B, \bar{\mu}_I\}$. For $x = \bar{\mu}_B$ we obtain

$$\bar{n}_B = -\frac{\partial\bar{\Omega}}{\partial\bar{\mu}_B}\,, \tag{72}$$

which is a consistency check since it is the thermodynamic relation we expect (but gives no further information). For $x = \bar{\mu}_I$, we obtain an expression for the isospin density,

$$\bar{n}_I = -\frac{\partial\bar{\Omega}}{\partial\bar{\mu}_I} = \frac{1}{2}\Big[-(\kappa_1\sin\alpha - \kappa_2\cos\alpha)\sin\theta + \kappa_3\cos\theta\Big]\,, \tag{73}$$

which we shall employ below in our explicit calculation.

It remains to write down the conditions obtained from minimizing the free energy with respect to the parameters θ, h_c, h_{3c}. Setting $x = \theta$ and requiring the derivative of $\bar{\Omega}$ with respect to θ to vanish, we read off of Eq. (67)

$$0 = \frac{1}{2}\Big[(\kappa_1\sin\alpha - \kappa_2\cos\alpha)\cos\theta + \kappa_3\sin\theta\Big] + \frac{2\bar{m}_\pi^2}{9\pi\bar{\mu}_I}\sin\theta\,. \tag{74}$$

From the stationarity of the free energy with respect to $x \in \{h_c, h_{3c}\}$ we obtain two conditions which, assuming $h_c, h_{3c} \neq 0$, can be written as

$$A_c = \frac{u_{\rm KK}^2 h_{(1)}}{2\sqrt{3}\lambda_0 h_c h_{3c}}\,, \tag{75a}$$

$$h_c h_{(1)} = h_{3c}h_{3(1)}\,. \tag{75b}$$

The three conditions (74), (75a), (75b) supplement the equations of motion (61), (62) and have to be solved simultaneously with them. We will explain our numerical procedure to do so at the beginning of Sec. 5.

Finally, we use the results just derived to write $\bar{\mu}_B$ and $\bar{\Omega}$ in a convenient form for the numerical evaluation. From Eqs. (60) and (75a) we have

$$\bar{\mu}_B = A_c + \int_{u_{\rm KK}}^{\infty} du\, A'(u) = \frac{u_{\rm KK}^2 h_{(1)}}{2\sqrt{3}\lambda_0 h_c h_{3c}} + \int_{u_{\rm KK}}^{\infty} du\,\frac{\bar{n}_B Q}{u^{5/2}\sqrt{f}}\,. \tag{76}$$

	$h_{1,2}(z)$	$h_3(z)$	$K_{1,2}(z)$	$K_3(z)$	θ	n_B	n_I
V	0	0	0	const	0	0	0
π	0	0	×	const	×	0	×
$\pi\rho$	0	×	×	const	×	0	×
ρ	×	0	0	const	0	0	×
B	×	×	0	×	0	×	×
πB	×	×	×	×	×	×	×

Table 1: Summary of the phases discussed in Sec. 4 in terms of the spatial and temporal non-abelian gauge components $h_{1,2}$, h_3 and $K_{1,2}$, K_3, as well as charged pion condensate θ, baryon density n_B and isospin density n_I. A "×" means the corresponding quantity is non-zero (and non-constant in z in the case of the gauge components). The pion condensate is non-zero if and only if $K_{1,2}$ are non-zero. The baryon number n_B is non-zero if and only if $h_{1,2}$ and h_3 are nontrivial. Isospin number n_I sits in the asymptotic behaviors of $K_{1,2}$ and K_3. If $K_3 = \text{const}$ only $K_{1,2}$ contribute to n_I. Rho meson condensation is encoded in the functions h and h_3 and is included without symmetry distinction in the baryonic phases. All phases listed here appear in the phase diagram, except for the ρ phase, which only appears if pion condensation is ignored. A second $\pi\rho$ phase where $h_3 = 0$ and $h \neq 0$ does exist as a solution but turns out to be irrelevant for the phase structure and is not discussed in the text.

For the free energy, we employ partial integration and the equations of motion to first compute

$$\begin{aligned} &\int_{u_{\rm KK}}^{\infty} du\, \frac{u^{5/2}}{2\sqrt{f}}(f K_a' K_a' + g_3) = \frac{\bar{\mu}_I \bar{n}_I}{2} \\ &\frac{3\lambda_0}{4}\int_{u_{\rm KK}}^{\infty} du\, A(h^2 h_3)' = \bar{\mu}_B \bar{n}_B - \int_{u_{\rm KK}}^{\infty} du\, \frac{(\bar{n}_B Q)^2}{u^{5/2}\sqrt{f}}\,. \end{aligned} \tag{77}$$

Inserting this into Eq. (39) with the Lagrangian (50) we get

$$\bar{\Omega} = \int_{u_{\rm KK}}^{\infty} du \frac{u^{5/2}}{2\sqrt{f}}\left[g_1 + g_2 + \frac{(\bar{n}_B Q)^2}{u^5}\right] - \bar{\mu}_B \bar{n}_B - \frac{\bar{\mu}_I \bar{n}_I}{2} - \frac{2\bar{m}_\pi^2}{9\pi}(\cos\theta - 1)\,. \tag{78}$$

This free energy is structurally identical to the one derived in Ref. [39], except for the additional mass term.

4 Different phases

There are various different configurations that solve our equations of motion, corresponding to different thermodynamic phases. These are summarized in Table 1. In the following we define these phases and discuss their physical content.

4.1 Vacuum (V) and pion-condensed phase (π)

In the vacuum, baryon and isospin densities vanish. The pion condensate is zero, $\theta = 0$, and all relevant functions are constants,

$$h(u) = h_3(u) = K_1(u) = K_2(u) = 0\,, \qquad A(u) = \bar{\mu}_B\,, \qquad K_3(u) = \frac{\bar{\mu}_I}{2}\,. \tag{79}$$

The free energy has been normalized such that it vanishes in this case, $\bar{\Omega} = 0$.

The pion-condensed phase was already discussed in Sec. 2.3. It is recovered as a solution of our more general setup for

$$h(u) = h_3(u) = 0\,, \qquad A(u) = \bar{\mu}_B\,, \tag{80}$$

while the functions $K_a(u)$ are given by Eq. (45). The pion condensate, free energy, and isospin density are given in Eq. (47). In the chiral limit, $m_\pi = 0$, this phase reduces to the pion-condensed configuration considered in Ref. [39]. In the given setup (confined geometry and maximally separated flavor branes) the holographic π phase is identical to what is obtained from lowest-order chiral perturbation theory.

4.2 Coexisting pion and rho meson condensates ($\pi\rho$) and rho meson phase (ρ)

Our motivation to introduce non-zero spatial components of the non-abelian gauge fields h and h_3 was to describe baryonic matter. We now demonstrate that due to the difference in h and h_3 our approach also enables us to include the physics of rho mesons, thus connecting our work with the analysis performed originally in Ref. [46].

Consider a configuration where $h(u) = 0$, but $h_3(u)$ is non-zero. On account of Eq. (55) this configuration has zero baryon number. Assuming a non-zero pion condensate, we simplify the calculation of the gauge potentials $K_a(u)$ by defining

$$\tilde{K}_1(u) = -\frac{2K_1(u)}{\bar{\mu}_I \sin\theta \sin\alpha}\,, \qquad \tilde{K}_2(u) = \frac{2K_2(u)}{\bar{\mu}_I \sin\theta \cos\alpha}\,, \qquad \tilde{K}_3(u) = \frac{2K_3(u)}{\bar{\mu}_I \cos\theta}\,. \tag{81}$$

The advantage of these new fields is that their boundary values are constant, irrespective of the (unknown) value of the pion condensate, $\tilde{K}_1(\infty) = \tilde{K}_2(\infty) = \tilde{K}_3(\infty) = 1$, which simplifies the numerical evaluation. The equations of motion (61a), (61b) and the boundary conditions (44a), (44b) are then the same for $\tilde{K}_1$ and $\tilde{K}_2$, and we can simply set

$$\tilde{K}_1(u) = \tilde{K}_2(u) \equiv \tilde{K}(u)\,, \tag{82}$$

which corresponds to $K_1(u)\cos\alpha + K_2(u)\sin\alpha = 0$. Since $h = 0$, Eq. (61c) yields the same $K_3(u)$ as in the π phase, which implies

$$\tilde{K}_3(u) = 1\,, \tag{83}$$

and it remains to solve (numerically) the system

$$(u^{5/2}\sqrt{f}\tilde{K}')' = \frac{\lambda_0^2 \tilde{K} h_3^2}{u^{1/2}\sqrt{f}}\,, \tag{84a}$$

$$(u^{5/2}\sqrt{f}h_3')' = -\frac{\bar{\mu}_I^2 \sin^2\theta \lambda_0^2 \tilde{K}^2 h_3}{u^{1/2}\sqrt{f}} \tag{84b}$$

for $\tilde{K}$ and h_3. Due to $h(u) = 0$ we have $h_c = h_{(1)} = 0$. Hence, from Eq. (67) we see that stationarity with respect to h_c is automatically fulfilled, while stationarity with respect to h_{3c} yields

$$h_{3(1)} = 0\,, \tag{85}$$

i.e., the slope of the function $h_3(z)$ vanishes at $z = 0$.

The isospin density is computed from Eq. (73) with the help of Eqs. (69) and (81), and can be written as

$$\bar{n}_I = \bar{\mu}_I X \sin^2\theta\,, \tag{86}$$

with the abbreviation

$$X \equiv \frac{\sqrt{3}u_{\rm KK}^2}{8}\tilde{K}_{(1)} + \frac{\lambda_0^2}{4}\int_{u_{\rm KK}}^{\infty} du \frac{\tilde{K}h_3^2}{u^{1/2}\sqrt{f}}\,. \tag{87}$$

This quantity also appears in the stationarity condition with respect to θ (74), which becomes

$$\cos\theta = \frac{\bar{m}_\pi^2}{\bar{\mu}_I^2}\frac{2}{9\pi X}\,. \tag{88}$$

In the π phase, the isospin density receives a contribution only from the first term in X. Now, in the presence of h_3, there is a second contribution. Also, the difference in the spatial components $A_3 \sim h_3 \neq 0$ and $A_{1,2} \sim h = 0$ renders the system anisotropic. We interpret this phase as rho meson condensation on top of the pion condensate and refer to it as the $\pi\rho$ phase. Indeed, Eqs. (84) are identical to Eqs. (4.21) in Ref. [46], where the rho meson condensate was sitting in the $\tau_{1,2}$ sector, as expected from a charged rho meson condensate in the usual frame. Here, due to our rotation (12) a τ_3 component of the charged rho meson is generated, which is accounted for by h_3. We can further confirm the equivalence to the results of Ref. [46] by discussing the continuous connection to the π phase. It is obvious from Eqs. (84a) and (88) that in the $h_3 \to 0$ limit $\tilde{K}$ and the pion condensate reduce to their solution in the pure π-phase,

$$\tilde{K}(z) = \frac{2}{\pi}\arctan\frac{z}{u_{\rm KK}}\,, \qquad \cos\theta = \frac{\bar{m}_\pi^2}{\bar{\mu}_I^2}\,. \tag{89}$$

Now, if we are in the $\pi\rho$ phase, h_3 is non-zero and approaches zero as we approach the transition point to the π phase. To find this point we employ Eq. (84b). We consider $\tilde{h}_3 = h_3/h_{3c}$ in order to work with a non-zero function with fixed boundary value $\tilde{h}_3(z = 0) = 1$. We also have $\tilde{h}_3'(z = 0) = 0$ due to Eq. (85), which holds for arbitrarily small values of h_{3c}. Also defining $\tilde{z} = z/u_{\rm KK}$ and using Eq. (89), we can write Eq. (84b) close to the transition point – but within the $\pi\rho$ phase – as

$$\tilde{h}_3'' + \frac{2\tilde{z}}{1+\tilde{z}^2}\tilde{h}_3' \;=\; -\frac{16\Lambda\tilde{h}_3\arctan^2\tilde{z}}{9\pi^2 u_{\rm KK}(1+\tilde{z}^2)^{4/3}}\,, \tag{90}$$

where prime is now the derivative with respect to $\tilde{z}$, and where

$$\Lambda \equiv \lambda_0^2\bar{\mu}_I^2\left(1 - \frac{\bar{m}_\pi^4}{\bar{\mu}_I^4}\right)\,. \tag{91}$$

For the given boundary conditions, Eq. (90) gives a tower of eigenvalues $\Lambda \simeq 1.90176$, $6.48327, 13.8360, 23.9705, \ldots$. For fixed model parameters λ, $\bar{m}_\pi$, these values translate into a critical chemical potential for the onset of a particular vector meson mode within the background of the pion condensate. We will only consider isospin chemical potentials large enough for the first, $\Lambda_1 = 1.90176$, but not for any higher mode to appear. In any case, at chemical potentials which allow for more than one vector meson to condense one would have to take into account the possibility of the coexistence of several condensates, while Eq. (91) only indicates the critical point for condensation of a single mode in the pionic background. Therefore, the relevant chemical potential is

$$\rho \text{ onset in pion condensate:} \qquad \bar{\mu}_I = \sqrt{\frac{\Lambda_1 + \sqrt{\Lambda_1^2 + 4\lambda_0^4\bar{m}_\pi^4}}{2\lambda_0^2}} \simeq \frac{\sqrt{\Lambda_1}}{\lambda_0}\,, \tag{92}$$

where the approximation holds for $m_\pi^2 \ll \Lambda M_{\rm KK}^2/2$. Since in our physical results we will choose $M_{\rm KK}$ to be of the order of 1 GeV, this is a good approximation.

The critical chemical potential (92) can be interpreted as the value of the effective rho meson mass (at that particular $\bar{\mu}_I$) in the pionic medium. It is therefore useful for comparison to also derive the vacuum mass of the rho meson within our setup. To this end, we switch off the pion condensate, $\theta = 0$, which allows us to set $K_1(u) = K_2(u) = 0$ due to the boundary conditions (44). Now, since in the absence of a pion condensate the rotation (12) is trivial, the rho meson condensate *does* sit in the $\tau_{1,2}$ sector. Therefore, we set $h_3 = 0$ and work with a non-zero h. The only non-trivial equations of motion are then Eqs. (61c) and (62a), which have to be solved numerically for K_3 and h. For our present purpose, we are again interested in the onset of rho meson condensation, this time in the vacuum, where $h = 0$. To this end, we can simply set $h = 0$ on the right-hand side of Eq. (61c) and find $\tilde{K}_3(u) = 1$. For Eq. (62a) we define $\tilde{h} = h/h_c$ to work with a non-zero and constant boundary value $\tilde{h}(z = 0) = 1$ to write this equation as

$$\tilde{h}'' + \frac{2\tilde{z}}{1+\tilde{z}^2}\tilde{h}' = -\frac{4\Lambda^{(0)}\tilde{h}}{9u_{\rm KK}(1+\tilde{z}^2)^{4/3}}\,, \tag{93}$$

with $\Lambda^{(0)} \equiv \lambda_0^2\bar{\mu}_I^2$. Once again, we compute the eigenvalues numerically, $\Lambda^{(0)} \simeq 0.669314$, $2.87432, 6.59117, 11.7967, \ldots$. Equation (93) is identical to Eq. (4.4) in the original work by Sakai and Sugimoto [7], which describes vector and axial vector mesons in the WSS model (our boundary conditions select the vector mesons). The lowest mode, $\Lambda_1^{(0)} = 0.669314$, corresponds to the ρ meson, and the corresponding critical chemical potential can be interpreted as the vacuum mass of the rho meson,

$$\bar{m}_\rho^2 = \frac{\Lambda_1^{(0)}}{\lambda_0^2}\,, \qquad m_\rho = \lambda_0 M_{\rm KK}\bar{m}_\rho\,, \tag{94}$$

where we have introduced the same notation for the dimensionless and dimensionful versions of the ρ mass as for the pion mass. We can thus express the critical chemical potential for the onset of rho meson condensation in the pionic background (92) in terms of the vacuum mass,

$$\bar{\mu}_I = \left[\sqrt{\frac{\Lambda_1}{\Lambda_1^{(0)}}} + \mathcal{O}\left(\frac{m_\pi^4}{m_\rho^4}\right)\right]\bar{m}_\rho \simeq 1.68\,\bar{m}_\rho\,. \tag{95}$$

Hence, the model predicts that the pionic medium increases the rho meson mass. The numerical factor is in agreement with Ref. [46], where the chiral limit was considered.

4.3 Baryonic matter (B)

Next, we consider the baryonic phase without pion condensate. We expect this phase to be relevant for baryon chemical potentials much larger than the isospin chemical potential. Since $\sin\theta = 0$ in this case, we can set $K_1(u) = K_2(u) = 0$. On the other hand, h and h_3 must both be non-vanishing to generate baryon number. Hence, in the B phase we need to solve the following equations of motion,

$$\partial_u(u^{5/2}\sqrt{f}\tilde{K}_3') = \frac{2\lambda_0^2\tilde{K}_3h^2}{u^{1/2}\sqrt{f}}\,, \tag{96a}$$

$$\partial_u(u^{5/2}\sqrt{f}h') - \frac{3\lambda_0 h h_3\bar{n}_B Q}{u^{5/2}\sqrt{f}} = \frac{\lambda_0^2 h}{u^{1/2}\sqrt{f}}\left(h^2 + h_3^2 - \bar{\mu}_I^2\tilde{K}_3^2\right)\,, \tag{96b}$$

$$\partial_u(u^{5/2}\sqrt{f}h_3') - \frac{3\lambda_0 h^2\bar{n}_B Q}{u^{5/2}\sqrt{f}} = \frac{2\lambda_0^2 h_3 h^2}{u^{1/2}\sqrt{f}}\,. \tag{96c}$$

The isospin density (73) assumes the form

$$\bar{n}_I = \frac{\bar{\mu}_I}{2}\lambda_0^2 \int_{u_{\rm KK}}^{\infty} \frac{du\, \tilde{K}_3 h^2}{u^{1/2}\sqrt{f}}\,. \tag{97}$$

Upon setting $h = h_3$ one recovers the B phase of Ref. [39]. Here, any non-zero μ_I produces *deformed* baryons with $h \neq h_3$, and the B phase can be continuously connected to the ρ phase discussed in the previous subsection. In the ρ phase, since $h_3 = 0$ and $h \neq 0$, we have $h_{3(1)} = 0$ while $h_c \neq 0$. These conditions, inserted into the stationarity condition for h_{3c} from Eq. (67), yield $A_c = 0$. With $\bar{n}_B = 0$ and Eq. (76), this implies $\bar{\mu}_B = 0$. Therefore, the B phase can connect continuously to the pure ρ phase only for vanishing baryon chemical potential,

$$\text{baryon onset in } \rho\text{:} \qquad \bar{\mu}_B = 0\,. \tag{98}$$

The B phase can also connect continuously to the vacuum. Letting both h and h_3 go to zero in Eqs. (96), the right-hand sides of Eqs. (96a) and (96c), as well as the terms proportional to $\bar{n}_B$ and the contribution $h^2 + h_3^2$ in Eq. (96b) are of higher order and can be neglected. One arrives at Eq. (93), which gives the critical isospin chemical potential $\bar{\mu}_I = \bar{m}_\rho$. Since h and h_3 go to zero, both stationarity conditions for h_c and h_{3c} from Eq. (67) are trivially fulfilled and thus there is no condition for A_c. As a consequence, this second-order onset does not depend on $\bar{\mu}_B$ and is a vertical line in the μ_B-μ_I phase diagram. In fact, as the full numerical calculation shows, this onset occurs in a metastable regime and is only realized in the phase diagram if pion condensation is omitted.

4.4 Baryonic matter coexisting with a pion condensate (πB)

This is the most complicated case since all functions are non-trivial and we have non-vanishing pion condensate, baryon density, and isospin density. We employ the redefined gauge potentials (81) and may set $\tilde{K}_1(u) = \tilde{K}_2(u) \equiv \tilde{K}(u)$ to solve the equations of motion (61) and (62), which now read

$$(u^{5/2}\sqrt{f}\tilde{K}')' = \frac{\lambda_0^2 \tilde{K}(h^2 + h_3^2)}{u^{1/2}\sqrt{f}}\,, \tag{99a}$$

$$(u^{5/2}\sqrt{f}\tilde{K}_3')' = \frac{2\lambda_0^2 \tilde{K}_3 h^2}{u^{1/2}\sqrt{f}}\,, \tag{99b}$$

$$(u^{5/2}\sqrt{f}h')' - \frac{3\lambda_0 h h_3 \bar{n}_B Q}{u^{5/2}\sqrt{f}} = \frac{\lambda_0^2 h}{u^{1/2}\sqrt{f}}\left[h^2 + h_3^2 - \bar{\mu}_I^2\left(\frac{\tilde{K}^2}{2}\sin^2\theta + \tilde{K}_3^2\cos^2\theta\right)\right]\,, \tag{99c}$$

$$(u^{5/2}\sqrt{f}h_3')' - \frac{3\lambda_0 h^2 \bar{n}_B Q}{u^{5/2}\sqrt{f}} = \frac{\lambda_0^2 h_3}{u^{1/2}\sqrt{f}}\left(2h^2 - \bar{\mu}_I^2 \tilde{K}^2 \sin^2\theta\right)\,. \tag{99d}$$

Obviously, by the redefinition (81) the pion condensate appears in the equations of motion themselves rather than in the boundary conditions. The isospin density (73) can be written as

$$\bar{n}_I = \bar{\mu}_I\left(X\sin^2\theta + \frac{\lambda_0^2}{2}\int_{u_{\rm KK}}^{\infty}\frac{du\,\tilde{K}_3 h^2}{u^{1/2}\sqrt{f}}\right)\,, \tag{100}$$

with

$$X \equiv \frac{\sqrt{3}u_{\rm KK}^2}{8}\tilde{K}_{(1)} + \frac{\lambda_0^2}{4}\int_{u_{\rm KK}}^{\infty}\frac{du}{u^{1/2}\sqrt{f}}\left[\tilde{K}(h^2 + h_3^2) - 2\tilde{K}_3 h^2\right]\,. \tag{101}$$

Expressed in terms of X, the stationarity condition of the free energy with respect to the pion condensate (74) becomes the same as in the $\pi\rho$ phase,

$$\cos\theta = \frac{\bar{m}_\pi^2}{\bar{\mu}_I^2}\frac{2}{9\pi X}\,. \tag{102}$$

Just like in the $\pi\rho$ phase, the pion condensate of the π phase (and chiral perturbation theory), $\cos\theta = \bar{m}_\pi^2/\bar{\mu}_I^2$, is corrected by a medium dependent term. Here, this term includes the effect of baryons and of rho meson condensation. We see from Eq. (102) that in the chiral limit, $\bar{m}_\pi = 0$, the pion condensate is maximal, irrespective of the medium (we have checked numerically that X remains finite in the chiral limit). In the presence of a pion mass, Eq. (102) yields an expression for the critical isospin chemical potential for the onset of a pion condensate within baryonic matter. Namely, upon setting $\cos\theta = 1$, thus assuming a second-order onset,

$$\text{pion onset in B:} \qquad \bar{\mu}_I^2 = \bar{m}_\pi^2\frac{2}{9\pi X}\,. \tag{103}$$

We shall indeed find that there is a region in the phase diagram where this second-order onset is realized. The specific value for the critical isospin chemical potential at a given baryon chemical potential – and thus the medium-dependent pion mass – has to be computed numerically.

As the B phase connects continuously to the ρ phase, the πB phase connects continuously to the $\pi\rho$ phase. To describe this transition, we need to take the limit $h(u) \to 0$. We can set $h = 0$ in Eqs. (99a), (99b), (99d), and these equations form a closed system for the functions $\tilde{K}$, $\tilde{K}_3$, and h_3, which are exactly the equations of the $\pi\rho$ phase discussed in Sec. 4.2. The onset of baryons is obtained with the help of Eq. (99c). We replace $h = h_c\tilde{h}$ and take the limit $h_c \to 0$ to obtain

$$(u^{5/2}\sqrt{f}\tilde{h}')' = \frac{\lambda_0^2\tilde{h}}{u^{1/2}\sqrt{f}}\left[h_3^2 - \bar{\mu}_I^2\left(\frac{\tilde{K}^2}{2}\sin^2\theta + \cos^2\theta\right)\right]\,, \tag{104}$$

where we have used $\tilde{K}_3 = 1$. Inserting the (numerical) solutions for $\tilde{K}$ and h_3 from the $\pi\rho$ phase, this can be solved for $\tilde{h}(u)$ with boundary condition $\tilde{h}(z=0) = 1$ [and $\tilde{h}(\infty) = 0$]. Now, the baryon chemical potential from Eq. (76) becomes, setting $\bar{n}_B = 0$,

$$\text{baryon onset in } \pi\rho\text{:} \qquad \bar{\mu}_B = \frac{u_{\rm KK}^2}{2\sqrt{3}\lambda_0}\frac{\tilde{h}_{(1)}}{h_{3c}}\,. \tag{105}$$

This is the critical chemical potential for a second-order onset of baryons within the $\pi\rho$ phase, where h_{3c} is computed within the $\pi\rho$ phase and $\tilde{h}_{(1)}$ is determined from solving Eq. (104). In contrast to the baryon onset in the ρ phase, see Eq. (98), the onset in the presence of a pion condensate (105) occurs at a non-zero (and $\bar{\mu}_I$ dependent) $\bar{\mu}_B$.

4.5 Neutron star matter

We may use our setup to address the question whether pion condensation takes place in neutron stars. To this end, we add a (non-interacting) lepton gas of electrons and muons, impose electric charge neutrality and equilibrium with respect to the electroweak interaction. Following Refs. [39, 40], this can be done in the B phase by assigning electric charges 0 and +1 to the two isospin components, i.e., by interpreting baryon and isospin densities to be composed of neutron and proton densities, although neutron and proton states are not explicitly present in our calculation. When meson condensates are added,

it is no longer obvious in our setup how to assign the electric charges because baryonic and mesonic contributions arise from the same gauge fields in the bulk. However, it will turn out not to be necessary to include pions – let alone rho mesons – here: in contrast to Refs. [39, 40] we have included a non-zero pion mass and thus we can check whether (and will confirm that) neutron star conditions are fulfilled in the B phase in a region where there is no stable solution of the πB phase.

Due to the different convention for the isospin chemical potential compared to Refs. [39, 40] it is useful for clarity to briefly recapitulate the conditions of electroweak equilibrium and neutrality. We define (dimensionless) neutron and proton chemical potentials by

$$\bar{\mu}_n = \bar{\mu}_B + \frac{\bar{\mu}_I}{2}\,, \qquad \bar{\mu}_p = \bar{\mu}_B - \frac{\bar{\mu}_I}{2}\,, \tag{106}$$

and (dimensionless) neutron and proton densities by

$$\bar{n}_n = \frac{\bar{n}_B}{2} + \bar{n}_I\,, \qquad \bar{n}_p = \frac{\bar{n}_B}{2} - \bar{n}_I\,. \tag{107}$$

Electroweak equilibrium with respect to the processes $p+e \to n+\nu_e$, $n \to p+e+\bar{\nu}_e$ reads

$$\mu_e = N_c \lambda_0 M_{\rm KK}(\bar{\mu}_n - \bar{\mu}_p) = N_c \lambda_0 M_{\rm KK} \bar{\mu}_I\,, \tag{108}$$

where μ_e is the (dimensionful) electron chemical potential and we have neglected the neutrino chemical potential. We also assume equilibrium with respect to purely leptonic processes converting an electron into a muon, such that electron and muon chemical potentials are identical, $\mu_e = \mu_\mu$. Due to electric charge neutrality, the proton density must be the same as the lepton density, which we can write as

$$\frac{\bar{n}_B}{2} - \bar{n}_I = \frac{3\pi^2}{\lambda_0^2 M_{\rm KK}^3}[n_e(\mu_e) + n_\mu(\mu_e)]\,, \tag{109}$$

where the (dimensionful) lepton densities are

$$n_\ell(\mu_\ell) = \Theta(\mu_\ell - m_\ell)\frac{(\mu_\ell^2 - m_\ell^2)^{3/2}}{3\pi^2}\,, \tag{110}$$

with $\ell = e, \mu$, electron mass $m_e \simeq 511\,\text{keV}$, and muon mass $m_\mu \simeq 106\,\text{MeV}$. Condition (109) has to be solved simultaneously with the relevant equations of the B phase in Sec. 4.3.

5 Numerical evaluation

In this section we evaluate the phases introduced in the previous section. Except for the π phase, whose analytical solutions were already discussed in Sec. 2.3, this has to be done numerically. We start by explaining our numerical procedure. For concreteness, we do so for the most complicated case, the πB phase, the other configurations are treated similarly and more easily. The main difference to Ref. [39] in the practical calculation is, besides the larger number of functions, the determination of the pion condensate. As in Ref. [39], the most straightforward calculation is to consider fixed $\bar{\mu}_I$ and $\bar{n}_B$ and compute $\bar{\mu}_B$ and $\bar{n}_I$ after solving the differential equations. The difference in these quantities is that $\bar{\mu}_I$ and $\bar{n}_B$ appear in the boundary conditions while $\bar{\mu}_B$ and $\bar{n}_I$ are given by the non-trivial expressions (76) and (100), which require the solution of the equations of motion. When we need to work at fixed $\bar{\mu}_B$ and/or $\bar{n}_I$ – for example to determine the preferred phase at a fixed point

in the $\bar{\mu}_B$-$\bar{\mu}_I$ phase diagram – we need to add Eq. (76) and/or Eq. (100) to the equations of motion. Here, we explain the simpler case where $\bar{\mu}_I$ and $\bar{n}_B$ are fixed. In addition to fixing these thermodynamic quantities, we also need to fix the model parameters $\bar{m}_\pi$ and λ (for the solution in terms of our dimensionless quantities, the third model parameter $M_{\rm KK}$ does not have to be fixed). The specific choice of the model parameters is discussed in Sec. 5.1.

We deal with the stationarity equation for the pion condensate by defining the auxiliary function

$$\xi(u) \equiv \int_{u_{\rm KK}}^{u} \frac{dv}{v^{1/2}\sqrt{f}} \left[\tilde{K}(h^2+h_3^2) - 2\tilde{K}_3 h^2\right] . \tag{111}$$

By definition, this function obeys the first-order differential equation

$$\xi'(u) = \frac{\tilde{K}(h^2+h_3^2) - 2\tilde{K}_3 h^2}{u^{1/2}\sqrt{f}} , \tag{112}$$

with boundary condition $\xi(u_{\rm KK}) = 0$. The pion condensate (102) can then be written purely in terms of boundary values/derivatives because

$$X = \frac{\sqrt{3}u_{\rm KK}^2}{8}\tilde{K}_{(1)} + \frac{\lambda_0^2}{4}\xi(\infty) . \tag{113}$$

We need to solve a system of 5 coupled differential equations – the equations of motion (99) and Eq. (112) – for the 5 functions $\tilde{K}$, $\tilde{K}_3$, h, h_3, ξ. We found it numerically advantageous to work in the z variable on one half of the connected flavor branes. More precisely, we use $\tilde{z} = z/u_{\rm KK}$ with $\tilde{z} \in [0,\infty]$. The calculation can be set up as an initial value problem with initial conditions at $\tilde{z} = 0$ (prime denoting derivative with respect to $\tilde{z}$)

$$\begin{gathered}\tilde{K}(0) = 0 , \quad \tilde{K}'(0) = p_1 , \quad \tilde{K}_3(0) = p_2 , \quad \tilde{K}_3'(0) = 0 , \quad \xi(0) = 0 \\ h(0) = p_3 , \quad h'(0) = p_4 , \quad h_3(0) = -\frac{4\bar{n}_B}{3\lambda_0 p_3^2} , \quad h_3'(0) = -\frac{3\lambda_0}{4\bar{n}_B} p_3^3 p_4 ,\end{gathered} \tag{114}$$

where we have introduced the variables p_1, p_2, p_3, p_4, and where we have expressed the initial conditions of h_3 in terms of $\bar{n}_B$, $h(0)$, and $h'(0)$ with the help of Eqs. (55) and (75b). Also, to make all unknowns explicit, we denote the boundary value $\xi(\infty)$ by p_5. We formulate the initial value problem in *Mathematica* with the help of *ParametricNDSolve* for the parameters $\bar{\mu}_I, \bar{n}_B, p_1, p_2, p_3, p_4, p_5$ and perform the actual calculation via *FindRoot*, solving the set of 5 equations

$$\tilde{K}(\infty) = 1 , \quad \tilde{K}_3(\infty) = 1 , \quad h(\infty) = 0 , \quad h_3(\infty) = 0 , \quad p_5 = \xi(\infty) , \tag{115}$$

for the 5 variables p_1, p_2, p_3, p_4, p_5. This determines the solutions $\tilde{K}$, $\tilde{K}_3$, h, h_3, ξ, which can then straightforwardly be used to compute $\cos\theta$, $\bar{\mu}_B$, $\bar{n}_I$, and the free energy density $\bar{\Omega}$ (78).

This procedure can be employed for the thermodynamic properties of the various phases but also for the phase diagram in the $\bar{\mu}_B$-$\bar{\mu}_I$ plane. To this end, the phase with lowest free energy has to be determined for each pair $(\bar{\mu}_B, \bar{\mu}_I)$. It is very tedious to compute the free energy for all possible phases in a sufficiently fine grid in the $\bar{\mu}_B$-$\bar{\mu}_I$ plane. Therefore, we set up specific calculations for the first-order phase transition curves, which simultaneously solves for the two phases that coexist on such a line supplemented by the condition that their free energies be the same. The relevant second-order transitions can also be computed directly along the lines already discussed in the previous section for the specific phases. The resulting phase diagram – the main result of our paper – is shown in Fig. 1 and discussed in Sec. 1. It includes the curve in the μ_B-μ_I plane for neutron star matter, where we have added the constraints of Sec. 4.5. For this phase diagram we have matched our parameters to QCD properties as we discuss now.

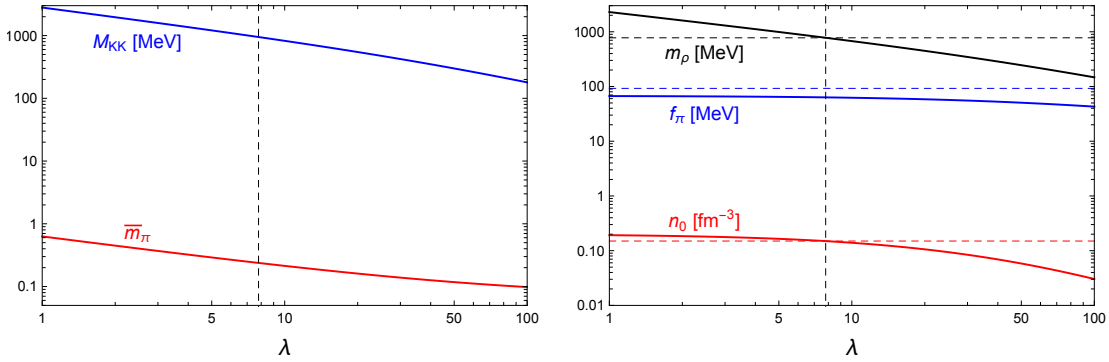

Figure 2: *Left panel:* Kaluza-Klein mass $M_{\rm KK}$ and dimensionless pion mass $\bar{m}_\pi$ as functions of λ given by the matching conditions (116). *Right panel:* Vacuum mass of the rho meson m_ρ, pion decay constant f_π, and saturation density of isospin-symmetric nuclear matter n_0 as functions of λ resulting from $M_{\rm KK}$ of the left panel. The horizontal dashed lines are the corresponding physical values. The vertical dashed line in both panels marks $\lambda = 7.8$, the value chosen for our main results, which reproduces the correct m_ρ and n_0, but leads to a deviation from the physical value of f_π.

5.1 Parameter fit

The parameters of our model are the Kaluza-Klein scale $M_{\rm KK}$, the 't Hooft coupling λ and the pion mass, say in its dimensionless form $\bar{m}_\pi$. Since our main result is the phase diagram in the μ_B-μ_I plane, it makes sense to anchor our results to the locations of the phase transitions on the two axes that are known from QCD. On the μ_B axis, there is a first-order onset of isospin-symmetric nuclear matter at a critical quark chemical potential $\mu_0 \simeq 308\,\text{MeV}$. On the μ_I axis, there is a second-order onset of pion condensation at $\mu_I = m_\pi$. We already know that this is reproduced in our model, and thus matching this transition amounts to reproducing the physical pion mass $m_\pi \simeq 140\,\text{MeV}$. Hence we require

$$\lambda_0 M_{\rm KK} \bar{\mu}_B = \mu_0\,, \qquad \lambda_0 M_{\rm KK} \bar{m}_\pi = m_\pi\,, \tag{116}$$

where $\bar{\mu}_B$ is the chemical potential at the baryon onset, which needs to be calculated numerically. Other basic quantities that our model should ideally reproduce are the saturation density of nuclear matter, i.e., the baryon density at μ_0, which is known to be $n_0 \simeq 0.15\,\text{fm}^{-3}$, the pion decay constant $f_\pi \simeq 92.4\,\text{MeV}$, and the vacuum mass of the rho meson $m_\rho \simeq 776\,\text{MeV}$. Obviously, with our 3 parameters we cannot fit these 5 values exactly. We proceed with the following observation. The dimensionless chemical potential $\bar{\mu}_B$ in Eq. (116) assumes different values for different values of λ, but does not depend on $M_{\rm KK}$ [it also does not depend on $\bar{m}_\pi$ since there are no terms of the form $m_\pi n_B$ in our effective action, see discussion below Eqs. (51)] . As a consequence, Eq. (116) fixes $M_{\rm KK}$ and $\bar{m}_\pi$ as functions of λ, shown in the left panel of Fig. 2. With these functions at hand, we can compute n_0 (numerically), f_π [from Eq. (34)], and m_ρ [from Eq. (94)] as functions of λ, see right panel of Fig. 2.

We see that in this approach we have to live with an unphysical pion decay constant, no matter which λ we choose. This tension between fitting vacuum properties and properties of nuclear matter simultaneously in the WSS model is known [36, 40]. We also see that, interestingly, by an appropriate choice of λ we can fit *two* more quantities to good accuracy, namely n_0 and m_ρ. This motivates our physical parameter choice for the phase diagram

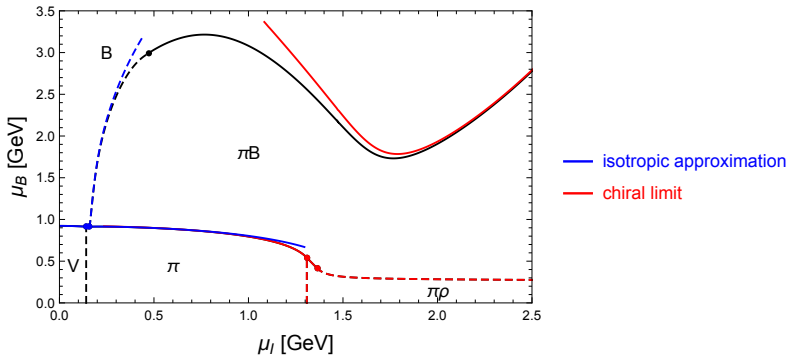

Figure 3: Comparison of our calculation within the diagonal ansatz (black curves, same as in Fig. 1) with the isotropic approximation (blue curves) and the chiral limit $m_\pi = 0$ (red curves). The black baryon onset curves (transitions from V, π, $\pi\rho$ to B and πB) are completely covered by one (or both) of these limits.

in Fig. 1 and for the results in the following subsections:

$$M_{\rm KK} = 949\,{\rm MeV}\,, \qquad \bar{m}_\pi = 0.24\,, \qquad \lambda = 7.8\,. \tag{117}$$

The (unphysical) value of the pion decay constant for this choice is $f_\pi = 63.6\,{\rm MeV}$.

5.2 Validity of the diagonal approximation

We have pointed out that our diagonal ansatz (49) is not a consistent solution of the full equations of motion, see text below this ansatz. Having set up our numerical evaluation, we are now in the position to test the validity of our approximation. To this end, we consider the phase diagram in the μ_B-μ_I plane and employ the two limits mentioned below Eq. (49).

Firstly, we re-compute the phase transition lines at small μ_I in the isotropic approximation, which we know is a consistent solution to the equations of motion at $\mu_I = 0$. More precisely, we assume that the only non-zero spatial gauge components in the Lagrangian (28) are the diagonal components $h \equiv h_1 = h_2 = h_3$ and derive the equations of motion under this constraint, i.e., for the single function h and the usual temporal components of the gauge fields. (This reproduces the approach of Ref. [39], but with a non-zero pion mass and thus a dynamical pion condensate.) Of course, this approach does not yield a fully consistent solution for $\mu_I > 0$ either. The idea is rather to identify the regions in the phase diagram where our baryonic matter is approximately isotropic: in the regions where the isotropic approximation is in good agreement with our diagonal, but anisotropic, approach, we can expect that the full anisotropic approach does not differ much from the solution we have found. In Fig. 3 we show the isotropic approximation (blue curves) in comparison with our phase transition lines from Fig. 1 (black curves). We see that in the lower left corner of the phase diagram the two sets of lines are basically indistinguishable (the pion onset from the vacuum is irrelevant for this comparison since it does not involve any spatial components of the gauge fields). Expected deviations occur in the pion onset within baryonic matter as μ_B is increased and in the baryon onset within the pion-condensate phase as μ_I is increased.

The second limit we show in Fig. 3 is the chiral limit $m_\pi = 0$. In this limit, the full equations of motion *are* fulfilled without any off-diagonal components for arbitrary anisotropy in the diagonal components. This is best seen by employing the rotation of

Refs. [39, 46, 58], i.e., $g_R = \mathbb{1}$, $g_L = \Sigma_0^\dagger$, instead of the rotation (12), which is more conveniently employed in the physical case. As explained below Eq. (12), the rotation $g_R = \mathbb{1}$, $g_L = \Sigma_0^\dagger$ does not generate τ_1 and τ_2 components if applied to the isospin chemical potential in the τ_3 component. Therefore, two of the non-abelian temporal gauge fields can be set to zero, which is sufficient to also keep the off-diagonal spatial components switched off. Since we expect the chiral limit to be a good approximation for $\mu_I \gg m_\pi$, we have re-computed the phase transition lines in that regime setting $m_\pi = 0$ (red curves). For low baryon chemical potentials, we see that the curves are indistinguishable from our $m_\pi > 0$ results. One can check from the analytical expression for the critical chemical potential of the π-$\pi\rho$ transition (92) that the pion mass gives a correction smaller than 0.01 % to the location of this transition Perhaps more surprisingly, the chiral limit also approximates the π-πB transition very well, essentially all the way down to the pion mass (where the red curve is covered by the blue curve), despite the pion condensate being far from maximal as $\mu_I \to m_\pi$. However, inclusion of the pion mass does result in a stronger deviation from the chiral limit in the πB-B transition. (The red curve for this transition is expected to diverge for $\mu_I \to 0$, as in this regime baryonic matter becomes isotropic, and the πB phase is always preferred [39].)

Taking the results of the two limits together, the main conclusion from Fig. 3 is as follows. The agreement of our diagonal, anisotropic, non-zero m_π approximation with the red and blue curves gives us confidence that our approximation works well in sizable regions of the phase diagram at small and large μ_I and even for all μ_I if μ_B is not too large. Our ansatz provides an interpolation between these two limits which is strictly speaking uncontrolled since we have dropped the off-diagonal components of the gauge fields. However, Fig. 3 suggests that – given the isotropic and chiral limits – there is not much room left for any additional structure other than what our ansatz yields. Therefore, the qualitative shape of our phase diagram seems to be a robust prediction.

5.3 Anisotropy in the baryonic phases

We have just seen with the help of the phase transition lines that the baryonic phases (B and πB) are isotropic to a good approximation for small μ_I. Due to rho meson condensation the anisotropy will become more significant for large μ_I. In Fig. 4, we show the extent of the anisotropy quantitatively. To this end, we have plotted the ratio $r(z) = h_3(z)/h(z)$ for the B and πB phases at various points (μ_B, μ_I), which, to facilitate the interpretation, we have marked in the phase diagram reproduced above the plots. For two of the points, there is no solution for the πB configuration (no blue solid lines in the middle and right panels), while solutions for both configurations exist at all other selected points, although, of course, at least one of the two phases is only metastable for a given point. The first general observation is that the numerical value of this ratio differs significantly between the infrared and ultraviolet regimes, $z \to 0$ and $z \to \infty$. For the following interpretation we may either focus on the infrared or on the ultraviolet, the main conclusions are the same.

For both B and πB phases, we see that the anisotropy is relatively small for the smallest isospin chemical potential used here, as expected from the comparison with the isotropic approximation in the previous subsection. Note that this "small" μ_I is already larger than the maximal μ_I found in neutron stars (constructed from our model). As expected, the anisotropy tends to get larger as μ_I is increased at fixed μ_B or as μ_B is decreased at fixed μ_I. The purely baryonic phase, i.e., the B phase, has values of $r(z)$ which are smaller than 1 everywhere. The reason is that this phase "wants" to turn into the ρ phase, where $h_3 = 0$ and the rho meson condensate sits in the first two components in flavor space, i.e., in h. In contrast, in the extreme anisotropic limit the πB phase "wants" to turn into the

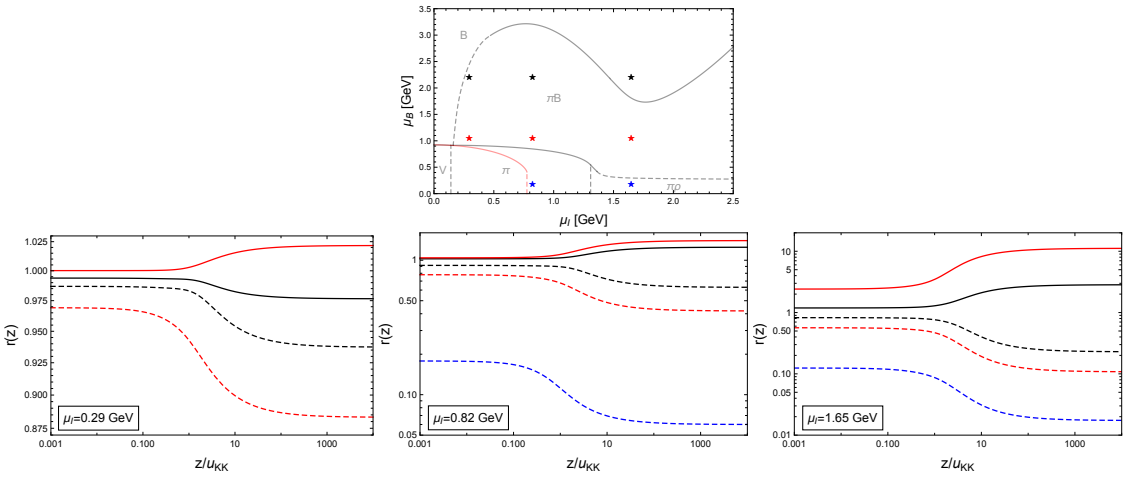

Figure 4: Ratio of the spatial components of the non-abelian gauge fields $r(z) = h_3(z)/h(z)$ for the πB phase (solid lines) and the B phase (dashed lines) for different values of μ_I and in each panel $\mu_B = 2.21\,(\text{black}), 1.06\,(\text{red}), 0.18\,(\text{blue})$ GeV. All points (μ_I, μ_B) are indicated in the phase diagram, which is reproduced from Fig. 1. Note the difference in vertical scales in the three panels; the anisotropy [deviation of $r(z)$ from 1] increases strongly from left to right, interpreted as a larger admixture of a rho meson condensate.

$\pi\rho$ phase, where $h = 0$ and the ρ meson condensate sits in h_3. [For the location of this transition see Eq. (105).] Hence we expect $r(z) > 1$, which is indeed the case except for a small region close to the B-πB transition (see black solid line in the left panel).

It might be tempting to translate these results into phase transition lines marking the onset of rho meson condensation within each of the baryonic phases. However, the results show that these transitions are not very sharp (at least for the physical value of the 't Hooft coupling chosen here). Perhaps one can argue that in the B phase the jump from the black to the red curves is much smaller than that of the red to the blue curve in both middle and right panels, and thus this transition is, roughly speaking, horizontal in the phase diagram. In the πB phase a similar argument (not immediately obvious from the curves shown here) suggests a more vertical transition. In any case, since in our approximation rho meson condensation in baryonic matter does not break any additional symmetries, there is no rigorous criterion for the transition and we do not attempt to add any phase transition lines to the phase diagram. We have, instead, included labels ρB and $\pi\rho$B in Fig. 1 to indicate the approximate locations of these baryonic phases with a rho meson admixture.

5.4 Thermodynamic properties

We discuss the physical properties of the various phases by plotting the densities n_B, n_I and the pion condensate $\sin\theta$ in Figs. 5 and 6. These figures are best understood as vertical and horizontal cuts through the phase diagram in Fig. 1, with the cuts chosen such that all features of the phase diagram can be understood and interpreted with the help of Figs. 5 and 6. We collect the main observations in the following list.

- *Thermodynamic consistency.* Following the stable phases for increasing μ_I (μ_B), the corresponding density n_I (n_B) is either constant or increases, as it should. This includes first-order phase transitions, where the densities increase discontinuously.

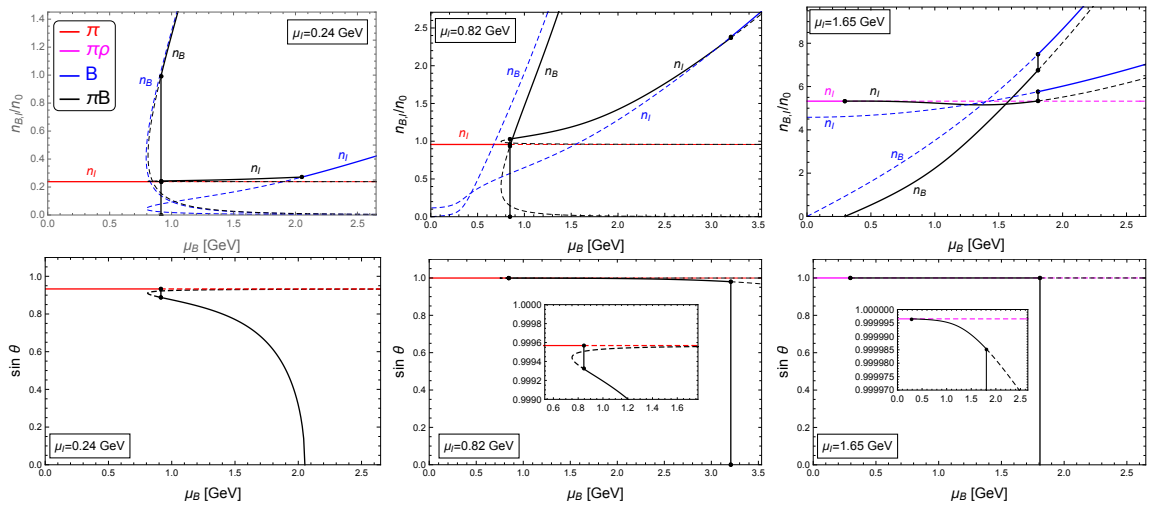

Figure 5: *Upper panels:* baryon and isospin densities in units of saturation density n_0 as a function of the baryon chemical potential for three different isospin chemical potentials. In each panel, all phases that are favored in at least one domain of the panel are shown. When they are favored, the corresponding curve is solid; unstable and metastable phases are shown as dashed curves. Different phases are distinguished by color, as given in the legend in the upper left panel. Discontinuities due to first-order phase transitions are marked with vertical (black) lines. *Lower panels:* Pion condensate for the same isospin chemical potentials as in the upper panels. In regions where the B phase is favored, the pion condensate is zero.

- *Onset of baryons.* At vanishing isospin chemical potential, the onset of baryons is at the physical value $\mu_B \simeq 923\,\mathrm{MeV}$ due to our parameter fit [recall that the chemical potential in Eq. (116) refers to the *quark* chemical potential, while the physical chemical potential μ_B used in all plots is the *baryon* chemical potential]. The upper row in Fig. 5 shows that the onset chemical potential decreases with increasing μ_I and eventually the onset becomes second order. We also find that, for sufficiently small μ_B and any μ_I, the baryonic phases are either metastable (B, blue curves) or do not even exist as a solution of the equations of motion (πB, black curves).

- *Pion condensate.* One of the novelties of our approach is the dynamical calculation of the pion condensate in the medium of holographic baryons. As discussed, in the π phase our results merely reproduce chiral perturbation theory, but all other phases with pion condensate (including the transition from the π phase to them) are a prediction of our holographic approach. The behavior is shown in the lower panels of Figs. 5 and 6. In Fig. 5 we observe that the pion condensate vanishes for sufficiently large baryon chemical potentials. In the lower left panel of Fig. 6 the inset shows the onset of rho meson condensation from the π phase. Interestingly, the pion condensate is larger compared to the (then metastable) pure pion-condensed phase. We also see in both Figs. 5 and 6 that the pion condensate is (either zero or) essentially maximal, $\sin\theta \simeq 1$, for $\mu_I \gtrsim 1\,\mathrm{GeV}$. This confirms the observation of Fig. 3 that the massless limit is a good approximation in this regime.

- *Rho meson condensation.* We have interpreted a large anisotropy in our gauge fields as a sign of rho meson condensation in baryonic matter. We can confirm

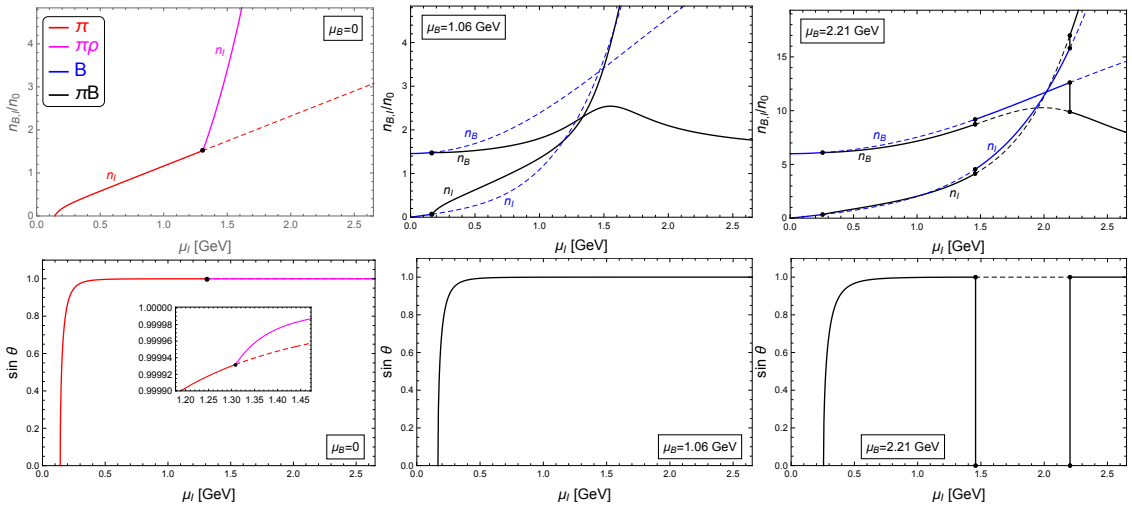

Figure 6: Same as Fig. 5, but as functions of the isospin chemical potential for three different values of the baryon chemical potential.

this interpretation now with the thermodynamic behavior. Let us first consider the baryon and isospin number densities in the B phase in the upper middle panel of Fig. 5 (blue curves). For small μ_B, this phase is metastable, nevertheless the behavior of n_B is instructive. We see that it is very small until it starts to increase rapidly at about $\mu_B \sim 300\,\mathrm{MeV}$. This suggests that for small μ_B it is mainly rho mesons that account for isospin number and that there is a rather sharp crossover to baryonic matter. For the πB phase, let us consider the densities in the upper middle panel of Fig. 6 (black curves). At large μ_I we find an interesting maximum of the baryon density. The system decides to remove baryons while the isospin density keeps increasing without qualitative change. Since the pion condensate is essentially maximal throughout this regime, the only possible interpretation is that a rho meson condensate now provides a large fraction of the isospin density. This corresponds to a large anisotropy of the gauge fields, cf. Fig. 4.

- *Disappearance and re-appearance of the pion condensate.* A surprising result in the phase diagram in Fig. 1 is the non-monotonic behavior of the first-order πB-B phase transition line. As a consequence, there is a region where, upon increasing μ_I at fixed μ_B, the pion condensate disappears, before re-appearing at even larger μ_I. This scenario is shown in the right panels of Fig. 6. A possible interpretation is that the system switches off the pion condensate because rho mesons become the more efficient way to generate isospin number. And, as we know at least from the case without baryons, the rho meson mass is larger in the presence of a pion condensate. Hence the rho meson condensate is less costly without the pions. This interpretation is supported by the observation that once rho mesons contribute significantly to the isospin density in the πB phase (judging from the decrease in n_B), this phase is again favored, i.e., the pion condensate re-appears. While Fig. 3 suggests that the non-monotonicity is not an artifact of our diagonal ansatz, we should keep in mind that we always work in the probe brane approximation, which becomes questionable if the gauge fields on the flavor branes are large. In particular, we have only considered the confined geometry and therefore our setup does not show a deconfinement or chiral phase transition, which is expected in QCD at very large chemical potentials. Also,

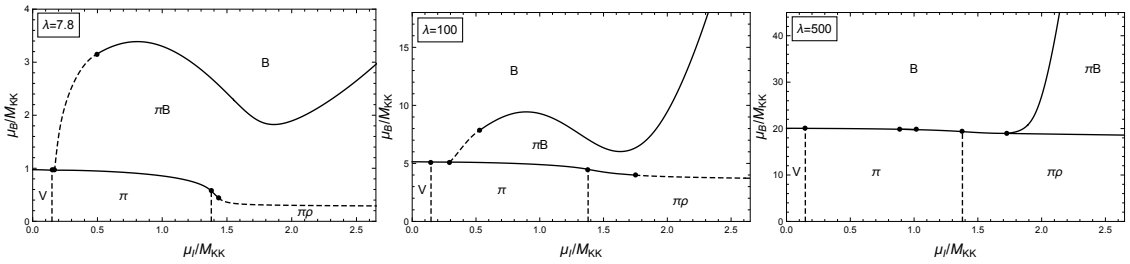

Figure 7: Phase diagram for three different values of the 't Hooft coupling and $\bar{m}_\pi$ chosen such that the ratio m_π/m_ρ is the same in each case and equal to its physical value. The left panel is identical to the physical phase diagram in Fig. 1, up to the dimensionless scales chosen here for all three panels, $\mu_B/M_{\rm KK} = N_c\lambda_0\bar{\mu}_B$, $\mu_I/M_{\rm KK} = \lambda_0\bar{\mu}_I$. The two dots on the π-B transition line in the right panel indicate a small πB pocket, narrower than the thickness of the line.

we find that the non-monotonicity disappears if the coupling strength is increased, as we demonstrate next.

5.5 Phase diagram at different coupling strengths

While our main physical result is the phase diagram with the specific parameter choice (117), it is instructive to study the dependence of our results under variation of the coupling strength λ. In particular, we may ask what the structure of the phase diagram is for large λ. This is the limit in which our classical gravity approximation is valid, while small values of λ (and N_c) rely, strictly speaking, on uncontrolled extrapolations. We have not found a direct way to compute the $\lambda \to \infty$ version of our phase diagram, but we have re-calculated the phase transition lines for the two additional values $\lambda = 100$ and $\lambda = 500$. By showing the results in units of $M_{\rm KK}$, this requires no specific choice of the Kaluza-Klein scale. However, the dimensionless pion mass parameter $\bar{m}_\pi$ cannot be scaled out of the equations and we need to decide how to readjust it upon variation of λ. From Eq. (94) we know that the rho meson mass m_ρ scales with λ^0, while the pion mass m_π scales with λ for fixed $\bar{m}_\pi$, see Eq. (36). Hence, if we kept $\bar{m}_\pi$ fixed, the rho meson would become lighter relative to the pion as we increase λ (and actually lighter than the pion for sufficiently large λ). For a sensible comparison, we therefore adjust $\bar{m}_\pi$ such that the ratio m_π/m_ρ keeps its physical value. This results in $\bar{m}_\pi \simeq 0.019, 0.0037$ for $\lambda = 100, 500$. The phase diagrams thus computed are shown in Fig. 7.

As a consequence of keeping the meson mass ratio fixed and choosing the isospin chemical potential in units of the Kaluza-Klein scale as the horizontal axis, the V $\to \pi$ and $\pi \to \pi\rho$ transitions at small baryon chemical potential occur at the same critical points in all three cases. The baryon onset at vanishing isospin chemical potential scales with the baryon mass (minus the binding energy of symmetric nuclear matter at saturation, which is different for each λ). Since the baryon mass scales with λ [74], the critical baryon chemical potential for the V $\to$ B transition thus increases from the left to the right panel.

The first main observation is that the phase transition lines that separate the purely mesonic phases from the phases containing baryons becomes more and more horizontal as the coupling strength is increased. In other words, the properties of the baryons seem to become essentially independent of the isospin chemical potential. This observation is in accordance with the properties of a single baryon at large λ. In this case, the BPST solution is, to leading order, unaffected by isospin (and baryon) chemical potentials, which

simply introduce non-trivial – sub-leading – temporal components of the gauge fields, see appendix A of Ref. [39]. We also see that the curious non-monotonicity of the B-πB transition disappears gradually for large λ. As a consequence, in the strongly coupled limit pion condensation in baryonic matter is restricted to a region of extremely large isospin chemical potentials. This is an interesting observation also for neutron star applications: if this tendency is of general value, the absence of a pion condensate in dense nuclear matter – which we observe even for the physical, less strongly coupled parameter set – may be interpreted as a strong-coupling effect.

Acknowledgements

We thank Mark Alford, Christian Ecker, Nick Evans, and Jack Mitchell for valuable discussions. The work of N.K. is supported by the ERC Consolidator Grant 772408-Stringlandscape. A.P. is supported by the National Research Foundation of Korea under the grants, NRF-2022R1A2B5B02002247, NRF-2020R1A2C1008497. N.K. and A.P. acknowledge the hospitality of the APCTP in Pohang, South Korea, where part of this work was developed.

References

[1] J. Kogut and D. Sinclair, *Quenched lattice QCD at finite isospin density and related theories*, Phys. Rev. D **66**, 014508 (2002), doi:10.1103/PhysRevD.66.014508, hep-lat/0201017.

[2] J. Kogut and D. Sinclair, *Lattice QCD at finite isospin density at zero and finite temperature*, Phys. Rev. D **66**, 034505 (2002), doi:10.1103/PhysRevD.66.034505, hep-lat/0202028.

[3] B. Brandt, G. Endrődi and S. Schmalzbauer, *QCD phase diagram for nonzero isospin-asymmetry*, Phys. Rev. D **97**(5), 054514 (2018), doi:10.1103/PhysRevD.97.054514, 1712.08190.

[4] B. B. Brandt, F. Cuteri and G. Endrődi, *Equation of state and Taylor expansions at nonzero isospin chemical potential*, PoS **LATTICE2022**, 144 (2023), doi:10.22323/1.430.0144, 2212.01431.

[5] B. B. Brandt, F. Cuteri and G. Endrődi, *Equation of state and speed of sound of isospin-asymmetric QCD on the lattice* (2022), 2212.14016.

[6] E. Witten, *Anti-de Sitter space and holography*, Adv. Theor. Math. Phys. **2**, 253 (1998), doi:10.4310/ATMP.1998.v2.n2.a2, hep-th/9802150.

[7] T. Sakai and S. Sugimoto, *Low energy hadron physics in holographic QCD*, Prog. Theor. Phys. **113**, 843 (2005), doi:10.1143/PTP.113.843, hep-th/0412141.

[8] T. Sakai and S. Sugimoto, *More on a holographic dual of QCD*, Prog. Theor. Phys. **114**, 1083 (2005), doi:10.1143/PTP.114.1083, hep-th/0507073.

[9] J. M. Maldacena, *The Large N limit of superconformal field theories and supergravity*, Adv.Theor.Math.Phys. **2**, 231 (1998), doi:10.1023/A:1026654312961, hep-th/9711200.

[10] E. Witten, *Anti-de Sitter space, thermal phase transition, and confinement in gauge theories*, Adv.Theor.Math.Phys. **2**, 505 (1998), hep-th/9803131.

[11] P. Kovtun, D. T. Son and A. O. Starinets, *Viscosity in strongly interacting quantum field theories from black hole physics*, Phys. Rev. Lett. **94**, 111601 (2005), doi:10.1103/PhysRevLett.94.111601, hep-th/0405231.

[12] J. Casalderrey-Solana, H. Liu, D. Mateos, K. Rajagopal and U. A. Wiedemann, *Gauge/String Duality, Hot QCD and Heavy Ion Collisions*, Cambridge University Press, ISBN 978-1-139-13674-7, doi:10.1017/CBO9781139136747 (2014), 1101.0618.

[13] C. Hoyos, D. Rodríguez Fernández, N. Jokela and A. Vuorinen, *Holographic quark matter and neutron stars*, Phys. Rev. Lett. **117**(3), 032501 (2016), doi:10.1103/PhysRevLett.117.032501, 1603.02943.

[14] E. Annala, C. Ecker, C. Hoyos, N. Jokela, D. Rodríguez Fernández and A. Vuorinen, *Holographic compact stars meet gravitational wave constraints*, JHEP **12**, 078 (2018), doi:10.1007/JHEP12(2018)078, 1711.06244.

[15] N. Jokela, M. Järvinen and J. Remes, *Holographic QCD in the Veneziano limit and neutron stars*, JHEP **03**, 041 (2019), doi:10.1007/JHEP03(2019)041, 1809.07770.

[16] K. Bitaghsir Fadafan, J. Cruz Rojas and N. Evans, *Deconfined, Massive Quark Phase at High Density and Compact Stars: A Holographic Study*, Phys. Rev. D **101**(12), 126005 (2020), doi:10.1103/PhysRevD.101.126005, 1911.12705.

[17] C. Ecker, M. Järvinen, G. Nijs and W. van der Schee, *Gravitational waves from holographic neutron star mergers*, Phys. Rev. D **101**(10), 103006 (2020), doi:10.1103/PhysRevD.101.103006, 1908.03213.

[18] P. M. Chesler, N. Jokela, A. Loeb and A. Vuorinen, *Finite-temperature Equations of State for Neutron Star Mergers*, Phys. Rev. D **100**(6), 066027 (2019), doi:10.1103/PhysRevD.100.066027, 1906.08440.

[19] K. Bitaghsir Fadafan, J. Cruz Rojas and N. Evans, *Holographic quark matter with colour superconductivity and a stiff equation of state for compact stars*, Phys. Rev. D **103**(2), 026012 (2021), doi:10.1103/PhysRevD.103.026012, 2009.14079.

[20] T. Demircik, C. Ecker and M. Järvinen, *Rapidly Spinning Compact Stars with Deconfinement Phase Transition*, Astrophys. J. Lett. **907**(2), L37 (2021), doi:10.3847/2041-8213/abd853, 2009.10731.

[21] N. Jokela, M. Järvinen, G. Nijs and J. Remes, *Unified weak and strong coupling framework for nuclear matter and neutron stars*, Phys. Rev. D **103**(8), 086004 (2021), doi:10.1103/PhysRevD.103.086004, 2006.01141.

[22] T. Demircik, C. Ecker and M. Järvinen, *Dense and Hot QCD at Strong Coupling*, Phys. Rev. X **12**(4), 041012 (2022), doi:10.1103/PhysRevX.12.041012, 2112.12157.

[23] H. Hata, T. Sakai, S. Sugimoto and S. Yamato, *Baryons from instantons in holographic QCD*, Prog. Theor. Phys. **117**, 1157 (2007), doi:10.1143/PTP.117.1157, hep-th/0701280.

[24] F. Brünner, J. Leutgeb and A. Rebhan, *A broad pseudovector glueball from holographic QCD*, Phys. Lett. **B788**, 431 (2019), doi:10.1016/j.physletb.2018.11.043, 1807.10164.

[25] F. Bigazzi and P. Niro, *Neutron-proton mass difference from gauge/gravity duality*, Phys. Rev. **D98**(4), 046004 (2018), doi:10.1103/PhysRevD.98.046004, 1803.05202.

[26] J. Leutgeb and A. Rebhan, *Witten-Veneziano mechanism and pseudoscalar glueball-meson mixing in holographic QCD*, Phys. Rev. D **101**(1), 014006 (2020), doi:10.1103/PhysRevD.101.014006, 1909.12352.

[27] F. Preis, A. Rebhan and A. Schmitt, *Inverse magnetic catalysis in dense holographic matter*, JHEP **1103**, 033 (2011), doi:10.1007/JHEP03(2011)033, 1012.4785.

[28] F. Preis, A. Rebhan and A. Schmitt, *Inverse magnetic catalysis in field theory and gauge-gravity duality*, Lect.Notes Phys. **871**, 51 (2013), doi:10.1007/978-3-642-37305-3_3, 1208.0536.

[29] O. Bergman, G. Lifschytz and M. Lippert, *Holographic Nuclear Physics*, JHEP **11**, 056 (2007), doi:10.1088/1126-6708/2007/11/056, 0708.0326.

[30] M. Rozali, H.-H. Shieh, M. Van Raamsdonk and J. Wu, *Cold Nuclear Matter In Holographic QCD*, JHEP **01**, 053 (2008), doi:10.1088/1126-6708/2008/01/053, 0708.1322.

[31] V. Kaplunovsky, D. Melnikov and J. Sonnenschein, *Baryonic Popcorn*, JHEP **11**, 047 (2012), doi:10.1007/JHEP11(2012)047, 1201.1331.

[32] S.-w. Li, A. Schmitt and Q. Wang, *From holography towards real-world nuclear matter*, Phys. Rev. **D92**(2), 026006 (2015), doi:10.1103/PhysRevD.92.026006, 1505.04886.

[33] F. Preis and A. Schmitt, *Layers of deformed instantons in holographic baryonic matter*, JHEP **07**, 001 (2016), doi:10.1007/JHEP07(2016)001, 1606.00675.

[34] M. Elliot-Ripley, P. Sutcliffe and M. Zamaklar, *Phases of kinky holographic nuclear matter*, JHEP **10**, 088 (2016), doi:10.1007/JHEP10(2016)088, 1607.04832.

[35] K. Bitaghsir Fadafan, F. Kazemian and A. Schmitt, *Towards a holographic quark-hadron continuity*, JHEP **03**, 183 (2019), doi:10.1007/JHEP03(2019)183, 1811.08698.

[36] N. Kovensky and A. Schmitt, *Holographic quarkyonic matter*, JHEP **09**, 112 (2020), doi:10.1007/JHEP09(2020)112, 2006.13739.

[37] H. Nishihara and M. Harada, *Equation of state in the pion condensation phase in asymmetric nuclear matter using a holographic QCD model*, Phys. Rev. D **90**(11), 115027 (2014), doi:10.1103/PhysRevD.90.115027, 1407.7344.

[38] T. Ishii, M. Järvinen and G. Nijs, *Cool baryon and quark matter in holographic QCD*, JHEP **07**, 003 (2019), doi:10.1007/JHEP07(2019)003, 1903.06169.

[39] N. Kovensky and A. Schmitt, *Isospin asymmetry in holographic baryonic matter*, SciPost Phys. **11**(2), 029 (2021), doi:10.21468/SciPostPhys.11.2.029, 2105.03218.

[40] N. Kovensky, A. Poole and A. Schmitt, *Building a realistic neutron star from holography*, Phys. Rev. D **105**(3), 034022 (2022), doi:10.1103/PhysRevD.105.034022, 2111.03374.

[41] N. Kovensky, A. Poole and A. Schmitt, *Predictions for neutron stars from holographic nuclear matter*, SciPost Phys. Proc. **6**, 019 (2022), doi:10.21468/SciPostPhysProc.6.019, 2112.10633.

[42] O. Aharony and D. Kutasov, *Holographic Duals of Long Open Strings*, Phys. Rev. **D78**, 026005 (2008), doi:10.1103/PhysRevD.78.026005, 0803.3547.

[43] K. Hashimoto, T. Hirayama, F.-L. Lin and H.-U. Yee, *Quark Mass Deformation of Holographic Massless QCD*, JHEP **07**, 089 (2008), doi:10.1088/1126-6708/2008/07/089, 0803.4192.

[44] R. McNees, R. C. Myers and A. Sinha, *On quark masses in holographic QCD*, JHEP **11**, 056 (2008), doi:10.1088/1126-6708/2008/11/056, 0807.5127.

[45] N. Kovensky and A. Schmitt, *Heavy Holographic QCD*, JHEP **02**, 096 (2020), doi:10.1007/JHEP02(2020)096, 1911.08433.

[46] O. Aharony, K. Peeters, J. Sonnenschein and M. Zamaklar, *Rho meson condensation at finite isospin chemical potential in a holographic model for QCD*, JHEP **02**, 071 (2008), doi:10.1088/1126-6708/2008/02/071, 0709.3948.

[47] A. B. Migdal, *Stability of Vacuum and Limiting Fields*, Soviet Journal of Experimental and Theoretical Physics **34**, 1184 (1972).

[48] R. F. Sawyer, *Condensed pi- phase in neutron star matter*, Phys. Rev. Lett. **29**, 382 (1972), doi:10.1103/PhysRevLett.29.382.

[49] D. J. Scalapino, *Pi- condensate in dense nuclear matter*, Phys. Rev. Lett. **29**, 386 (1972), doi:10.1103/PhysRevLett.29.386.

[50] A. B. Migdal, *Pi condensation in nuclear matter*, Phys. Rev. Lett. **31**, 257 (1973), doi:10.1103/PhysRevLett.31.257.

[51] G. Baym, *Pion condensation in nuclear and neutron star matter*, Phys. Rev. Lett. **30**, 1340 (1973).

[52] D. N. Voskresensky, *S-wave pion condensation in symmetric nuclear matter*, Phys. Rev. D **105**(11), 116007 (2022), doi:10.1103/PhysRevD.105.116007, 2201.07536.

[53] D. T. Son and M. A. Stephanov, *QCD at finite isospin density: From pion to quark - anti-quark condensation*, Phys. Atom. Nucl. **64**, 834 (2001), doi:10.1134/1.1378872, hep-ph/0011365.

[54] S. Carignano, L. Lepori, A. Mammarella, M. Mannarelli and G. Pagliaroli, *Scrutinizing the pion condensed phase*, Eur. Phys. J. A **53**(2), 35 (2017), doi:10.1140/epja/i2017-12221-x, 1610.06097.

[55] B. B. Brandt, G. Endrődi, E. S. Fraga, M. Hippert, J. Schaffner-Bielich and S. Schmalzbauer, *New class of compact stars: Pion stars*, Phys. Rev. D **98**, 094510 (2018).

[56] J. O. Andersen and M. K. Johnsrud, *Phases of QCD at nonzero isospin and strangeness chemical potentials with application to pion stars* (2022), 2206.04291.

[57] L. Bartolini and S. B. Gudnason, *Symmetry energy in holographic QCD* (2022), 2209.14309.

[58] A. Rebhan, A. Schmitt and S. A. Stricker, *Meson supercurrents and the Meissner effect in the Sakai-Sugimoto model*, JHEP **05**, 084 (2009), doi:10.1088/1126-6708/2009/05/084, 0811.3533.

[59] F. Preis, A. Rebhan and A. Schmitt, *Holographic baryonic matter in a background magnetic field*, J. Phys. G **39**, 054006 (2012), doi:10.1088/0954-3899/39/5/054006, 1109.6904.

[60] D. B. Kaplan and A. E. Nelson, *Strange Goings on in Dense Nucleonic Matter*, Phys. Lett. B **175**, 57 (1986), doi:10.1016/0370-2693(86)90331-X.

[61] A. Schmitt, *Dense matter in compact stars: A pedagogical introduction*, Lect. Notes Phys. **811**, 1 (2010), doi:10.1007/978-3-642-12866-0, 1001.3294.

[62] D. Son and M. A. Stephanov, *QCD at finite isospin density*, Phys. Rev. Lett. **86**, 592 (2001), doi:10.1103/PhysRevLett.86.592, hep-ph/0005225.

[63] J. B. Kogut and D. Toublan, *QCD at small nonzero quark chemical potentials*, Phys. Rev. D **64**, 034007 (2001), doi:10.1103/PhysRevD.64.034007, hep-ph/0103271.

[64] J. Gasser and H. Leutwyler, *Chiral Perturbation Theory to One Loop*, Annals of Phys. **158**, 142 (1984), doi:10.1016/0550-3213(83)90063-9.

[65] G. Ecker, *Chiral perturbation theory*, Prog. Part. Nucl. Phys. **35**, 1 (1995), doi:10.1016/0146-6410(95)00041-G, hep-ph/9501357.

[66] T. Brauner and N. Yamamoto, *Chiral Soliton Lattice and Charged Pion Condensation in Strong Magnetic Fields*, JHEP **04**, 132 (2017), doi:10.1007/JHEP04(2017)132, 1609.05213.

[67] G. W. Evans and A. Schmitt, *Chiral anomaly induces superconducting baryon crystal*, JHEP **09**, 192 (2022), doi:10.1007/JHEP09(2022)192, 2206.01227.

[68] P. C. Argyres, M. Edalati, R. G. Leigh and J. F. Vazquez-Poritz, *Open Wilson Lines and Chiral Condensates in Thermal Holographic QCD*, Phys. Rev. **D79**, 045022 (2009), doi:10.1103/PhysRevD.79.045022, 0811.4617.

[69] K. Hashimoto, T. Hirayama and D. K. Hong, *Quark Mass Dependence of Hadron Spectrum in Holographic QCD*, Phys. Rev. **D81**, 045016 (2010), doi:10.1103/PhysRevD.81.045016, 0906.0402.

[70] S. Seki and S.-J. Sin, *Chiral Condensate in Holographic QCD with Baryon Density*, JHEP **08**, 009 (2012), doi:10.1007/JHEP08(2012)009, 1206.5897.

[71] A. Belavin, A. M. Polyakov, A. Schwartz and Y. Tyupkin, *Pseudoparticle Solutions of the Yang-Mills Equations*, Phys. Lett. B **59**, 85 (1975), doi:10.1016/0370-2693(75)90163-X.

[72] G. S. Adkins, C. R. Nappi and E. Witten, *Static Properties of Nucleons in the Skyrme Model*, Nucl. Phys. B **228**, 552 (1983), doi:10.1016/0550-3213(83)90559-X.

[73] J. Cruz Rojas, T. Demircik and M. Järvinen, *Popcorn transitions and approach to conformality in homogeneous holographic nuclear matter*, Symmetry **15**(2), 331 (2023), doi:10.3390/sym15020331, 2301.03173.

[74] K. Hashimoto, T. Sakai and S. Sugimoto, *Holographic Baryons: Static Properties and Form Factors from Gauge/String Duality*, Prog. Theor. Phys. **120**, 1093 (2008), doi:10.1143/PTP.120.1093, 0806.3122.